Enalapril mitigates senescence and aging-related phenotypes by targeting antioxidative genes via phosphorylated Smad1/5/9

Wencong Lyu[1†], Haochen Wang[1†], Zhehao Du[1], Ran Wei[1], Jianuo He[1], Fanju Meng[1], Jinlong Bi[1], Lijun Zhang[1], Chao Zhang[2], Yiting Guan[3*] and Wei Tao[1*]

[1]The MOE Key Laboratory of Cell Proliferation and Differentiation, School of Life Sciences, Peking University, Beijing 100871, P. R. China

[2]Kunming Institute of Zoology, Chinese Academy of Sciences, Kunming 650201, P. R. China

[3]Zhanjiang Institute of Clinical Medicine, Central People's Hospital of Zhanjiang, Guangdong Medical University, Zhanjiang 524045, P. R. China

[†]These authors contributed equally to this work

[*]These authors jointly supervised this work

Correspondence:

Wei Tao (weitao@pku.edu.cn)

Yiting Guan (ytguan@pku.edu.cn)

ABSTRACT

Aging increases the risk of a myriad of chronic diseases, which are expensive and difficult to treat owing to their various risk factors. Repurposing existing medications has accelerated the development of therapies aimed at slowing aging. In this study, we revealed that enalapril, a drug widely prescribed for hypertension, can improve both cellular senescence and individual health. Mechanistically, phosphorylated Smad1/5/9 act as pivotal mediators of the anti-senescence properties of enalapril. It stimulates downstream genes involved in cell cycle regulation and antioxidative defense, facilitating cell proliferation and diminishing the production of reactive oxygen species (ROS), thus increasing the antioxidative ability of enalapril. At the organismal level, enalapril has been shown to bolster the physiological performance of various organs; it notably enhances memory capacity and renal function and relieves lipid accumulation. Our work highlights the potential of enalapril to augment antioxidant defenses and combat the effects of aging, thereby indicating its promise as a treatment strategy for aging-associated diseases and its use for healthy aging.

INTRODUCTION

Aging is a multifaceted process influenced by numerous factors, and its intricate mechanisms are not yet fully understood. Geroscience is a burgeoning field of study in which researchers hypothesize that aging is a significant risk factor for many chronic diseases. These findings suggest that interventions targeting the mechanisms of aging might delay the onset or slow the progression of these diseases(Kirkland, 2016; Lopez-Otin, Blasco, Partridge, Serrano, & Kroemer, 2023). Cellular senescence, a pivotal indicator of aging, is characterized by irreversible cell cycle arrest triggered by cellular damage or stress(Khosla, Farr, Tchkonia, & Kirkland, 2020). During cellular senescence, cells exhibit increased activity of the lysosomal enzyme senescence-associated β-galactosidase (SA-β-gal), decreased proliferation marker Ki67 signals and increased senescence-associated secretory phenotype (SASP) secretion(Coppe et al., 2008; Dimri et al., 1995).

Senescence is the result of a complex interplay of endogenous and exogenous signaling pathways(Cohen et al., 2022). Currently, the activation of tumor suppressor pathways, such as $p16^{INK4a}$/RB, is deemed essential for senescence-related cessation of proliferation(Baker et al., 2011). The disruption of signaling pathways disrupts tissue homeostasis, leading to proinflammatory responses that are increasingly recognized as fundamental aspects of senescence(Coppe et al., 2008; Shah et al., 2013). Researchers have suggested that the expression of p16 is suppressed by inhibitor of DNA-binding (ID) proteins. The expression of the *ID1* gene is downregulated by transforming growth factor-β (TGF-β), while it is upregulated by BMP-mediated phosphorylated SMAD signaling in various cell types(Hayashi et al., 2016; Liang, Brunicardi, & Lin, 2009). SMADs are crucial transcriptional effector factors responsible for transmitting TGF-β/BMP signals(Urist, 1965). They convey signals from the TGF-β superfamily and homomeric serine/threonine kinases on the cell surface to the nucleus, directly regulating transcriptional programs critical for key events(Miyazono, Maeda, & Imamura, 2005). Numerous studies have shown that the BMP-SMAD signaling pathway can modulate genes involved in the cell cycle, which affects the balance between cell proliferation and senescence(Genander et al., 2014; Hayashi et al., 2016).

Phosphorylated SMAD plays a crucial role in the induction and maintenance of pluripotency, helping maintain tissue homeostasis during aging(Orlowski, 2017). However, dysregulation of BMP signaling during aging can lead to fibrosis, impaired wound healing, or excessive tissue calcification, which are detrimental to tissue function(Lyu et al., 2018; Rahman, Akhtar, Jamil, Banik, & Asaduzzaman, 2015).

Owing to increasing insights into cellular and individual aging, novel aging mechanisms and signaling pathways have been identified, leading to the development of new therapeutic interventions. Senescent cells have recently been targeted in therapy given their substantial impact on aging (Childs et al., 2017). Consequently, eliminating senescent cells through pharmacological interventions, known as "senolytics", may delay the onset or slow the progression of age-related diseases and enhance physiological function(Childs et al., 2017). Research has proven that specific senolytic drugs, such as dasatinib and quercetin, can eliminate senescent cells, reverse aging phenotypes and increase the survival rate of mice(Xu et al., 2018; Zhu et al., 2015). However, the current senolytics are not universally effective across different cell types and display inconsistent sensitivities, thereby limiting their broad application(Yousefzadeh et al., 2018; Zhu et al., 2016). In addition to senolytics, researchers have explored pharmacological interventions that aim to ameliorate or reverse aging phenotypes without the need to eliminate senescent cells. This included both the repurposing of existing medications and the development of new ones(Bharath et al., 2020; Harrison et al., 2014). However, repurposing is particularly attractive due to its cost-effectiveness; these drugs have already undergone rigorous safety evaluations, allowing for quicker implementation in new contexts. For example, drugs such as metformin, which is typically used to treat type 2 diabetes, and rapamycin, an immunosuppressant, have shown promise in reducing aging phenotypes and extending the lifespan(Bharath et al., 2020; Harrison et al., 2009). This strategy is an innovative pharmacological intervention in which existing compounds target the aging process.

In this study, we employed a drug repurposing strategy to evaluate the anti-senescence potential of several FDA-approved drugs and identified enalapril as a promising candidate. Our investigation revealed that enalapril increases pSmad1/5/9

levels, which in turn upregulates key downstream genes involved in cell cycle regulation and antioxidative defense, thereby improving cell proliferation, reducing inflammation, and decreasing reactive oxygen species (ROS) levels. Our findings confirmed the anti-senescence mechanism of enalapril at both the cellular and organismal levels. Enalapril has the ability to ameliorate aging-related phenotypes of various organs, with notable effects on the brain, kidney, and liver. Furthermore, treating aged mice with enalapril improved spatial memory and anxiety behavior, alleviated lipid accumulation, and mitigated kidney aging-related phenotypes. Taken together, the potential of enalapril to extend the healthspan and ameliorate age-related diseases makes it a compelling candidate for research and development in the field of anti-aging therapeutics.

MATERIALS AND METHODS

Cell culture

IMR90 cells were cultured in DMEM (Gibco, C11995500) supplemented with 10% fetal bovine serum (Cellmax, SA111) and 1% non-essential amino acids (Gibco, 11140050) at 37°C and 5% CO_2. When the cell density in the in vitro culture reached 80–90% (usually within 2 or 3 days), cell passage was performed.

Drug preparation and addition

Enalapril (MCE, HY-B0331) was dissolved in DMSO to prepare a 10 mM stock solution. When used, it was diluted to 10 μM in the culture medium. After the cells adhered to the surface, enalapril was added for treatment, and RNA and protein were collected for analysis. Recombinant BMP4 protein (MCE, HY-P7007) was dissolved in sterile ddH_2O to prepare a 100 μg/mL stock solution. When used, it was diluted to 50 ng/mL in the culture medium and added to the cells. The BMP receptor inhibitor (LDN193189, MCE, HY-12071) was dissolved in sterile ddH_2O to prepare a 1 mM stock solution. When used, it was diluted to 1 μM or 0.5 μM in the culture medium. The ID inhibitor (Pimozide, MCE, HY-12987) was dissolved in DMSO to prepare a 10 mM stock solution. When used, it was diluted to 5 μM in the culture medium. After the cells

adhered to the surface, drugs were added for a 3-day treatment, and samples were collected for analysis.

Senescence-associated β-galactosidase (SA-β-gal) Staining

SA-β-gal staining was performed using a Senescence β-Galactosidase Staining Kit (Sigma–Aldrich, CAS0030). Briefly, 0.6×10^5 cells were seeded in a 6-well plate. The cells were fixed with fixation buffer and incubated at room temperature for 10 minutes. After the cells were washed three times with PBS, the prepared staining mixture was added to the 6-well plate, and the plate was incubated at 37°C overnight. The stained cells were observed and photographed under a microscope.

Western blot

Proteins were extracted using TRIzol reagent (Invitrogen, 15596018CN) and dissolved in 1% SDS, after which SDS–PAGE was performed. The samples were transferred to nitrocellulose membranes and incubated with 5% skimmed milk at room temperature for 30 minutes. The primary antibodies were incubated overnight at 4°C, followed by three washes with PBST. The membranes were then incubated with secondary antibody at room temperature for two hours. The band signals were visualized using an Odyssey Infrared Imaging System (Odyssey, LI-COR). All antibody information is provided in Table S4.

RT-qPCR

Total RNA from cultured cells was extracted using TRIzol reagent (Invitrogen, 15596018CN) according to the manufacturer's instructions. The DEPC-treated water-dissolved RNA was subsequently reverse transcribed into cDNA using the HiScript III All-in-one RT SuperMix Perfect for qPCR (Vazyme, R333) following the product manual. The cDNA levels of specific primers were analyzed using the LightCycler® 96 qPCR system (Roche), and the results were normalized to those of β-actin. The primers used in this analysis are listed in Table S1.

RNA-seq and data processing

Total RNA was extracted using TRIzol reagent (Invitrogen, 15596018CN) following the manufacturer's instructions. The extracted total RNA was then sent to Novogene for subsequent cDNA library construction. The library was sequenced with paired-end reads on the Illumina HiSeq PE150 platform.

For data processing, FastQC (version 0.11.5) software was first used for data quality control. Raw paired-end sequencing reads were trimmed by Trim Galore (version 0.6.10) software to remove adapter sequences and low-quality reads. The high-quality RNA-seq reads were mapped to the hg38/mm10 genome using HISAT2 (version 2.2.1) software(Kim, Paggi, Park, Bennett, & Salzberg, 2019). SAMtools (version 1.17) software was then used to convert the generated SAM files to bam files(Li et al., 2009). To qualify gene expression, the number of reads mapped to each gene was counted using featureCounts (version 2.0.1) software(Liao, Smyth, & Shi, 2014). Differentially expressed genes (DEGs) were calculated by R package DESeq2 (version 1.34.0)(Love, Huber, & Anders, 2014) with the cutoff values of Benjamini-Hochberg adjusted p-value < 0.05 and $|\log_2(\text{fold change})| > 0.5$. The gene expression count matrix was converted into the reads per kilobase per million mapped reads (RPKM) matrix, followed by Z score normalization for visualization.

CUT&Tag and data processing

For the CUT&Tag experiments, 8×10^5 cells were processed using the CUT&Tag Kit (Vazyme, TD903). The cells were collected and incubated with ConA beads and then mixed with the primary antibody pSmad1/5/9 (CST, #13820) overnight at 4°C. After incubation with the secondary antibody for one hour, the cells were further incubated with pA/G-Tnp for one hour. The transposase was then activated for DNA fragmentation. Following DNA extraction, library amplification and purification were performed. The libraries were sequenced using paired-end reads on the Illumina HiSeq PE150 platform.

For data processing, raw CUT&Tag data was trimmed using Trim Galore (version 0.6.10) software, and the clean reads were mapped to the human reference genome hg38 using Bowtie2 (version 2.5.1) software(Langmead & Salzberg, 2012) with the

following parameters: "--very-sensitive --no-mixed --no-discordant -I 10 -X 1000". The SAM files were transformed into bam files via SAMtools (version 1.17) software(Li et al., 2009). The CUT&Tag peaks were performed using the MACS2 (version 2.2.8) with the default parameters(Zhang et al., 2008). Differential peaks were calculated using the R package DiffBind (version 3.4.11) with the cutoff values of adjusted p-value < 0.05 and $|\log_2(\text{fold change})| > 0.5$ and annotated using the R package ChIPpeakAnno (version 3.28.0)(Lihua, Claude, & Nathan, 2010). To visualize the CUT&Tag signal, the reads per kilobase per million mapped reads (RPKM) were calculated in each 50-bp bin size using DeepTools (version 3.5.2) software(Ramirez, Dundar, Diehl, Gruning, & Manke, 2014), and the RPKM matrix was normalized using the Z score algorithm.

ChIP-qPCR

At room temperature, approximately 2×10^6 IMR90 cells were cross-linked with 1% paraformaldehyde for 10 minutes. The cross-linking reaction was stopped by adding 0.125 M glycine for 6 minutes. The cells were then harvested and lysed on ice in nuclear lysis buffer (50 mM Tris-Cl, 10 mM EDTA, 1% SDS, and protease inhibitors). Chromatin immunoprecipitation (ChIP) was performed using a Bioruptor (Diagenode) to shear the chromatin. Fragmented chromatin (25 μg) was immunoprecipitated with 5 μg of anti-pSmad1/5/9 antibody (CST, #13820) or anti-rabbit IgG (Abcam, ab171870). The immunoprecipitated DNA was quantified via RT-qPCR. The amount of DNA in the immunoprecipitates was calculated as a percentage relative to 10% of the input chromatin. All ChIP-qPCR-related primers are available in Table S2.

Immunofluorescence

The slides were washed twice in PBS, fixed with 4% PFA for 10 minutes, and washed again three times with PBS. Subsequently, permeabilization was performed via incubation with 0.5% Triton X-100 for 10 minutes, followed by three additional washes with PBS. Next, blocking was performed with 1% BSA, and after blocking, the slides were washed three times with PBS. The primary antibody (Ki67, Abcam, ab15580) was then diluted at a ratio of 1:500 in PBST (PBS + 0.1% Tween 20) and incubated overnight at 4°C. Afterward, the slides were washed four times with PBST, with each

189 wash lasting 5 minutes. The secondary antibody was diluted at a ratio of 1:500 in PBST
190 (1 × PBS + 0.1% Triton X-100) and incubated at room temperature for 1–1.5 hours.
191 After three washes with PBST, a final wash with PBS was conducted. DAPI was diluted
192 to a final concentration of 1–2 ng/μL and incubated at room temperature for 3–5 minutes.
193 Following three washes with PBS and one wash with ddH_2O, the slides were sealed
194 with Fluoromount-G® (SouthernBiotech, 0100-010) and covered with a coverslip.

195 **Lentiviral production and viral transduction**

196 First, the pLKO.1 empty vector or vectors encoding shRNAs targeting *ID1* or *ID2*
197 (Table S3), along with the assistant plasmids psPAX2 and pMD2.G, were cotransfected
198 into HEK293T cells. After 18 h of transfection, the medium was replaced with DMEM
199 supplemented with 30% complement-inactivated FBS, and viral supernatants were
200 collected after 24 h and 48 h of transfection. When IMR90 cells reached 70%
201 confluence, they were infected with the packaged virus with 5 μg/mL polybrene (MCE,
202 HY-K1057). At 36–48 hours after infection, successfully transduced cells were selected
203 via treatment with 1 μg/mL puromycin (M&C Gene Technology, MA009) for 24–36
204 hours.

205 **Detection of Reactive Oxygen Species (ROS)**

206 IMR90 cells were harvested from a 6-well plate. After the cells were washed, the ROS-
207 sensitive fluorescent probe 2',7'-dichlorofluorescin diacetate (DCFH-DA, MCE, HY-
208 D0940) was used for detection. A 10 mM stock solution of DCFH-DA was prepared by
209 dissolving it in anhydrous DMSO. This stock solution was subsequently diluted in
210 serum-free DMEM to obtain a 10 μM working solution of DCFH-DA. The samples
211 were incubated with the DCFH-DA probe at 37°C for 30 minutes. After incubation, the
212 samples were washed to remove excess probe. The fluorescence intensity was measured
213 via a fluorescence microscope. The fluorescence intensity corresponds to the level of
214 ROS present in the sample.

215 **Mice feeding**

216 All the mouse experiments were approved by the Institutional Animal Care and Use

Committee of Peking University. 12-month-old C57BL/6 mice (purchased from Wukong Biotech Co., Ltd.) were housed in a specific pathogen-free (SPF) animal facility under controlled environmental conditions with a temperature range of 20–25°C, 55±10% humidity, and a 12 h light/dark cycle. The mice had ad libitum access to food and water. A daily dosage of 30 mg/kg of enalapril was dissolved into the mice's drinking water. In the LDN treatment group, mice received intraperitoneal injections of the BMP receptor inhibitor LDN193189 (3 mg/kg, MCE, HY-12071) every other day. Four to ten mice were included in each group.

Forelimb grip strength test

The mice were placed on a grip strength meter, and their tails were gently pulled to allow them to grasp the pull bar with their forelimbs. The grip strength meter readings were recorded at the point of maximum force exerted by each mouse. The measurements were repeated multiple times to ensure reliable and consistent results.

Rotarod fatigue test

The mouse was placed on the rotarod, and rotation was initiated. The device was set to an accelerating mode that increased from 4 to 40 revolutions per minute over 300 seconds. The time at which each mouse fell off or lost balance was recorded. The test was repeated multiple times to assess the endurance and motor performance of the mice.

Y-maze test

The Y-maze consists of three opaque arms arranged at 120° angles relative to each other. The mice were placed in the central position of the maze and allowed to explore the three arms freely for 10 minutes. Each consecutive entry into one of the three arms was defined as spontaneous alternation behavior. The total number of arm entries and the number of spontaneous alternations were recorded. The percentage of spontaneous alternation behavior was then calculated.

Open field test

The mice were removed from their cages and placed in an open field, with the central

area designated. The mice were allowed to move freely within the open field for 10 minutes, and the number of times that they crossed the central area was recorded.

Mouse serum extraction and analysis

After the mice were anesthetized, blood (approximately 1 mL per mouse) was collected from the eyeballs. The blood was allowed to clot and settle at room temperature. The mixture was then centrifuged at 3,000 rpm for 20 minutes, and the upper clear layer, which was the serum, was collected. The serum was subsequently subjected to biochemical assays, including ALT, CREA, LDH, TG, LDL, and HDL tests.

Mouse tissue extraction

After the mice were euthanized, they were perfused with prechilled PBS until no blood was expelled. The heart, liver, spleen, kidney, brain, and muscle tissues were harvested. A portion of each tissue sample was used for RNA and protein extraction for sequencing and Western blot analysis, respectively, while another portion was fixed in 4% paraformaldehyde (PFA). The tissues were then subjected to either frozen or paraffin embedding. Various staining techniques, including β-galactosidase (β-gal) staining, periodic acid-Schiff (PAS) staining, Congo red staining, Sirius red staining, Oil Red O staining, and hematoxylin and eosin (H&E) staining, were performed.

Pathway enrichment analysis

Gene Ontology (GO) enrichment analysis was performed with Metascape(Zhou et al., 2019), and gene set enrichment analysis (GSEA) was performed with the R package ClusterProfiler (version 4.2.2)(Wu et al., 2021). Pathways with p values < 0.05 were considered significantly enriched. Representative terms were visualized with the ggplot2 (version 3.3.6) R package and ComplexHeatmap (version 2.10.0) R package(Gu, 2022).

Statistical analysis

The data are expressed as means ± SEMs. The data were analyzed via a two-tailed unpaired Student's t test. A p value < 0.05 was considered statistically significant.

RESULTS

Enalapril restrains cellular replicative senescence.

To identify drugs that are capable of delaying cellular senescence, we established an in vitro replicative senescence model using primary human embryonic lung fibroblasts (IMR90). Compared with young cells, long-term-cultured IMR90 cells presented a characteristic senescence phenotype, characterized by increased SA-β-gal staining, increased expression of the cell cycle arrest factors p16 and p21, and reduced expression of the proliferation marker Ki67 (**Fig. S1A–C**). Additionally, the release of SASP factors that significantly alter the cellular microenvironment, including the well-described factors *IL-1β*, *IL-6*, and *CXCL10,* has also been reported to increase the degree of senescence (**Fig. S1D**).

Employing a drug repurposing strategy, we discovered that enalapril, an antihypertensive medication, delayed senescence. Notably, enalapril treatment at various concentrations reduced SA-β-gal staining and increased Ki67 positivity in IMR90 cells (**Fig. 1A–B, D–E**). Western blot analysis confirmed a decrease in the senescence markers p16 and p21 with the optimal effect of 10 μM enalapril (**Fig. 1C**). To further analyze the effects of enalapril on transcriptome dynamics upon senescence entry, RNA-seq was performed across enalapril-treated cells at different concentrations. In general, we found that the expression of SASP genes decreased significantly (**Fig. 1F**). The expression of cell cycle arrest factors typically increased during senescence; however, the expression of these factors decreased after exposure to enalapril, whereas the expression of cell cycle genes related to cell proliferation increased upon treatment with enalapril at the optimal concentration of 10 μM (**Fig. 1F**). We therefore treated the cells with 10 μM enalapril via RT-qPCR and detected that many prominent SASP genes, such as *IL-1β and IL-6*, were significantly reduced compared with those in the control (**Fig. 1G**). Moreover, enalapril treatment increased the cell growth rate and delayed the transition to the growth arrest phase (**Fig. 1H**). Our comprehensive analysis underscores enalapril's potential as an anti-senescence agent, warranting further exploration for its role in combating cellular senescence.

The function of enalapril depends on phosphorylated Smad1/5/9.

Given the potential of enalapril to decelerate senescence, we screened several important targets of the senescence-related pathway to identify the underlying mechanism of senescence entry. We found that enalapril notably elevated the phosphorylation level of Smad1/5/9 without affecting Smad2/3 phosphorylation, effectively reversing the decline of pSmad1/5/9 levels in senescent cells, suggesting a possible role for the BMP-pSmad1/5/9 pathway (**Fig. 2A, Fig. S2A, B**). To validate the pathway alterations in the gene expression profile, GSEA confirmed that enalapril treatment increased BMP signaling (**Fig. 2B**). Concurrently, the level of the Smad4 protein, which is required for pSmad1/5/9 to enter the nucleus, also increased, suggesting that enalapril might facilitate the nuclear entry of pSmad1/5/9 and modulate downstream genes (**Fig. 2A**)(Guglielmi et al., 2021; Senft, Bikoff, Robertson, & Costello, 2019). Notably, the expression of Smad4 was reduced in senescent cells, supporting the notion that enalapril reverses senescence-associated defects in BMP signaling (Fig. S2B). To further assess the impact on gene regulation, we employed CUT&Tag analysis of pSmad1/5/9 and found that enalapril treatment increased the pSmad1/5/9 binding signals at the transcription start site (TSS) regions (**Fig. 2C**).

To explore the potential role of pSmad1/5/9 in anti-senescence mechanisms, we experimentally manipulated its levels by supplementing with BMP4 to increase pSmad1/5/9 levels, or by reducing it using the BMP receptor inhibitor LDN193189 (LDN) and shRNA-mediated knockdown of the BMP receptor BMPR1A. Our findings revealed that BMP4 increased pSmad5 levels, which correlated with decreased p16 and p21, reduced β-gal staining and increased Ki67 positivity, indicating a mitigated senescent phenotype (**Fig. S3A–C**). In contrast, when cells were treated with the BMP receptor inhibitor LDN or subjected to *BMPR1A* knockdown, the changes in pSmad1/5/9 levels and senescence markers were completely reversed, highlighting that the suppression of pSmad1/5/9 accelerates the progression of senescence (**Fig. S4A–G**).

Encouraged by the observed association between pSmad1/5/9 and senescence, we tested whether pSmad1/5/9 mediates the anti-senescence effects of enalapril by co-

330 treating with enalapril and either LDN or shRNA targeting *BMPR1A*. RNA-seq analysis
331 revealed that LDN upregulated SASP genes and downregulated cell cycle genes. On
332 the basis of these findings, the subsequent addition of enalapril did not reverse these
333 changes, which suggests that the anti-senescence function of enalapril relies on
334 pSmad1/5/9 (**Fig. 2D**). Furthermore, western blot results also revealed that in the
335 presence of LDN, neither enalapril nor BMP4 restored Smad1/5/9 phosphorylation or
336 the expression of p16 and p21 (**Fig. 2E**). Similarly, β-gal and Ki67 staining also
337 revealed that enalapril failed to counteract the senescence-promoting effects induced by
338 either LDN treatment or BMPR1A knockdown (**Fig. 2F, G, Fig. S4F, G**). Collectively,
339 these results indicate that elevated pSmad1/5/9 could increase the expression of critical
340 genes, thereby exerting a potent anti-senescence effect.

341 **pSmad1/5/9 modulates the cell cycle and SASP secretion by upregulating *ID1*.**

342 The ID family, which is recognized as a key downstream target of pSmad1/5/9, serves
343 as a biomarker for Smad1/5/9 phosphorylation levels(Genander et al., 2014; Hayashi et
344 al., 2016; Ramachandran et al., 2018; Sun et al., 2022; Ying, Nichols, Chambers, &
345 Smith, 2003). Coincidentally, we found that *ID1* was the top-ranked transcription factor
346 that pSmad1/5/9 bound to its promoter region via CUT&Tag analysis after enalapril
347 treatment (**Fig. 3A**). Moreover, IGV analysis confirmed that enalapril significantly
348 increased pSmad1/5/9 enrichment at the *ID1* promoter (**Fig. 3B**). Simultaneously, the
349 expression levels of both *ID1* and *ID2* were elevated (**Fig. 3C, D**). Conversely,
350 inhibiting pSmad1/5/9 with LDN or shRNA targeting BMPR1A led to decreased *ID1*
351 and *ID2* levels, confirming the regulatory link between pSmad1/5/9 and the ID family
352 (**Fig. 3E, Fig. S4D**). This finding indicated that the ID family was indeed a downstream
353 gene regulated by pSmad1/5/9, and the increase in ID1 induced by enalapril further
354 confirmed that enalapril could upregulate pSmad1/5/9 levels, thereby affecting the
355 expression of downstream genes.

356 Prior studies have indicated that the ID family can suppress p16 and p21
357 expression, thus inhibiting cell cycle arrest and delaying cellular senescence(Hayashi
358 et al., 2016; Lyden et al., 1999; Ying et al., 2003). This prompted us to examine ID

protein expression during senescence, where we observed a decrease in ID1 and ID2 levels (**Fig. S5A**). The knockdown of *ID1* and *ID2* via shRNA or an ID1 inhibitor resulted in a decreasing trend of ID1 or ID2 expression and a significant increase in p16 and p21 expression (**Fig. 3F, I**). In addition, while β-gal increased the proportion of positively stained cells, the Ki67 proliferation signal decreased nearly fourfold after the knockdown of *ID1* or *ID2*, resembling the changes observed during senescence (**Fig. S5B, C)**. Given that enalapril reduced SASP factors while LDN increased them, we investigated whether ID1, which acts as a transcriptional repressor downstream of pSmad1/5/9, could modulate SASP expression. Indeed, the expression of traditional SASP factors, such as *IL1β* and *IL6*, which decrease with enalapril treatment, significantly increased after *ID* knockdown (**Fig. 3G**). By overlapping the genes downregulated by enalapril with those upregulated upon *ID* knockdown, several SASP genes, as well as *CDKN2A* and *CDKN2B,* were identified (**Fig. 3H**). Consistent with these findings, we found that SASP factor expression also increased in *ID* knockout mouse bone marrow cells in previously reported data (**Fig. S5E**)(Fei et al., 2023). Importantly, *ID* knockdown did not affect pSmad1/5/9 levels, confirming that ID is a downstream effector of pSmad1/5/9, influencing the expression of genes such as p16, p21, and SASP-related genes (**Fig. 3J**).

After validating the prosenescence effects of *ID* through shRNA targeting *ID* or the use of small molecule inhibitors, we next examined whether the anti-senescence effects of enalapril are mediated by ID proteins. The continued addition of enalapril to these *ID*-knockdown cells did not significantly alter β-gal or Ki67 signals compared with those in the *ID*-knockdown group without enalapril, implying that the benefits of enalapril may be ID dependent (**Fig. 3K–L, Fig. S5D**). Taken together, these findings indicate that enalapril elevates pSmad1/5/9 levels, which in turn upregulate *ID1* expression. This dual action has two key implications: first, it confirms that enalapril can modulate the expression of pSmad1/5/9 downstream genes. Second, by upregulating *ID1*, enalapril can suppress the expression of p16, p21, and SASP-related genes, thereby potentially restoring cell proliferation and reducing the expression of inflammatory factors. These findings suggest that the anti-senescence mechanism of

389 enalapril involves the pSmad1/5/9-ID1 axis, highlighting a novel pathway for its
390 therapeutic effects on aging.

391 **Enalapril has antioxidative effects through pSmad1/5/9.**

392 Since an increase in pSmad1/5/9 after enalapril treatment was observed and
393 pSmad1/5/9 is a transcription factor, to understand the in-depth mechanism of enalapril
394 regulation, we further explored the downstream genes of pSmad1/5/9. Analysis of
395 CUT&Tag-upregulated peaks after enalapril treatment revealed that enalapril treatment
396 led to enrichment of pSmad1/5/9 in the GO pathway associated with DNA replication,
397 the cell cycle and the oxidative stress response, all of which are crucial for cell growth
398 (**Fig. 4A**). Moreover, transcriptome analysis revealed that the genes whose expression
399 increased after enalapril treatment were also enriched in pathways related to the
400 response to oxidative stress (**Fig. 4A**). Notably, genes upregulated by enalapril in
401 response to oxidative stress included antioxidative enzymes, electron transport chain
402 components and lipid oxidation inhibitors, with a significant increase in pSmad1/5/9 at
403 their TSS regions (**Fig. 4B, C**). Specifically, we also examined the promoter regions of
404 antioxidative genes, such as the antioxidative enzyme *PRDX5* and the lipid oxidation
405 inhibitor *TXN*, and found increased pSmad1/5/9 enrichment along with upregulated
406 gene expression (**Fig. 4D, F–H**). During cellular senescence, a decrease in these
407 antioxidative genes exacerbates oxidative stress, reduces energy metabolism, and
408 increases lipid oxidation, leading to the release of inflammatory cytokines (**Fig.
409 4E**)(Coppe et al., 2008).

410 It has been reported that changes in the expression of antioxidative genes can affect
411 the ROS level of cells; thus, we then used DCFH-DA probes to detect ROS levels in
412 cells(Coppe et al., 2008). The results revealed that cellular senescence increased ROS,
413 whereas enalapril slowed the increase in ROS, indicating its ability to upregulate
414 antioxidative genes and reduce ROS, thus affecting cellular senescence (**Fig. 4I**).
415 Importantly, the continued addition of BMP receptor inhibitors LDN reversed the
416 beneficial effects of enalapril on ROS and decreased pSmad1/5/9 enrichment at the
417 promoters of these antioxidative genes (**Fig. 4G, I**). Similarly, shRNA-mediated

knockdown of *BMPR1A* also led to decreased expression of antioxidative genes such as *PRDX5* and *TXN* (**Fig. S4D**). Collectively, these results reinforce the notion that enalapril promotes the upregulation of antioxidative genes through pSmad1/5/9, reduces ROS levels and alleviates oxidative stress, thus playing a crucial role in delaying senescence.

Enalapril upregulates pSmad1/5/9 and improves physiological function in mice.

Enalapril, which is known for its anti-senescence potential, was further investigated for its impact at the organ and individual levels in 12-month-old mice (**Fig. 5A**). After continuous feeding at a dosage of 30 mg/kg/day for 3 months, we conducted a comprehensive RNA-seq analysis of six key organs—brain, kidney, liver, heart, muscle, and spleen—to assess the impact of enalapril on the transcriptome. We found that enalapril induced organ-specific gene expression changes, thereby affecting the physiological functions of these genes. Moreover, GSEA revealed upregulated pathways related to forebrain and kidney development, long-chain fatty acid metabolism and other processes, indicating that enalapril has a beneficial effect on organ functions (**Fig. S6A**). Additionally, enalapril reduced the expression of SASP factors in multiple organs, particularly the CCL, CXCL, and MMP families (**Fig. 5B**). Serum SASP array analysis also revealed a decrease in the secretion of certain SASP proteins, such as CCL6, CCL11, CXCL13, IGFBP-1, and MMP3, suggesting that enalapril has anti-inflammatory effects in mice (**Fig. 5C**).

Given the known upregulation of pSmad1/5/9 levels and antioxidative genes in cellular models by enalapril, we measured Smad1/5/9 phosphorylation and the expression of the antioxidative genes *Txn1*, *Txn2*, and *Prdx5* in the tested organs. We observed increased pSmad1/5/9 levels, especially in the brain, kidney and liver, along with upregulated *Id1* and antioxidative genes, notably *Txn1* and *Txn2* (**Fig. 5D, Fig. S6B**). Further analysis of BMP signaling and antioxidative stress-related pathways in these organs revealed increased gene expression after enalapril treatment, indicating the activation of this pathway (**Fig. 5E**). Building on these findings, intraperitoneal injection of the BMP inhibitor LDN reversed the effects of enalapril. Specifically, SASP

factor levels in serum, which were reduced by enalapril, were significantly increased. Additionally, the elevated pSmad1/5/9 and antioxidative genes in the brain, kidney and liver were markedly downregulated upon LDN treatment (**Fig. S7A, B**). These findings align with our cellular findings, implying that enalapril enhance the pSmad1/5/9-antioxidative gene axis to increase organ physiological function and delay individual aging.

Enalapril alleviates aging-related behavior in naturally aged mice.

Building on our finding of pSmad1/5/9 activation and antioxidative genes upregulation in multiple organs, we further investigated the broader phenotypic effects of enalapril in mice. After three months of enalapril feeding, behavioral experiments, serum tests, and tissue section staining were performed. Notably, enalapril had no significant effect on body weight in the mice, suggesting that the drug has no overt toxic side effects (**Fig. 6A**). However, enalapril improved the decrease in age-related mobility, as evidenced by increased grip strength and extended time in the rotarod fatigue experiments, suggesting increased muscle strength and endurance (**Fig. 6D, E**).

During the aging process, the brain undergoes varying degrees of functional decline. To assess the impact of enalapril on brain function, we conducted Y-maze and open field tests. The Y-maze, which is frequently employed to assess short-term memory in mice by measuring spontaneous alternation as a marker of spatial working memory, indicates notable improvements. Under normal circumstances, mice prefer to explore new maze branches rather than return to previously visited branches. Several brain regions, including the hippocampus, septum, basal forebrain, and prefrontal cortex, contribute to this task, and the age-related decline in spontaneous alternation ability in mice is associated with degeneration or lesions in brain regions such as the hippocampus(Radulescu, Cerar, Haslehurst, Kopanitsa, & Barnes, 2021). Enalapril promoted a substantial increase in the rate of spontaneous alternation in the mice, indicating enhanced spatial memory (**Fig. 6B, C**). As aging progresses, anxiety-like behaviors often increase with age in mice(Radulescu et al., 2021). The open-field test, a valuable tool for assessing autonomous and exploratory behaviors in new

environments, demonstrated that enalapril increased the number of central area crossings, suggesting a reduction in aging-related anxiety (**Fig. 6F, G**). However, LDN treatment reversed the improvements in muscle endurance, spatial memory, and reduced anxiety behaviors conferred by enalapril (**Fig. S8A–F**). In conclusion, these results suggest that enalapril has the potential to mitigate the deterioration of various behavioral aspects associated with aging through the activation of pSmad1/5/9.

Enalapril ameliorates aging-related pathological changes in aged mice.

The results of these behavioral tests provided valuable insights. To further explore the effects of enalapril on pathological changes, our investigation was extended to serum analyses. This comprehensive analysis encompassed the evaluation of vital organ function, including the liver, kidneys, and heart, as well as an assessment of lipid content, specifically triglycerides (TGs), low-density lipoprotein cholesterol (LDL), and high-density lipoprotein cholesterol (HDL). After enalapril administration, there was no significant change in the serum alanine transaminase (ALT) level, indicating that no liver toxicity from enalapril occurred (**Fig. 6H**). Moreover, the level of creatinine (CREA), a key marker of kidney function, was significantly decreased in enalapril-treated mice, indicating potential functional recovery and improvement of renal function (**Fig. 6I**). A heart health indicator, lactate dehydrogenase (LDH), was also reduced, indicating a positive cardiac effect of enalapril (**Fig. 6J**). These findings underscore the multifaceted effects of enalapril on various physiological parameters, emphasizing its potential as a therapeutic intervention in aging-related conditions.

The transcriptomic data from the enalapril treatment group revealed an increase in long-chain fatty acid metabolism in the liver, suggesting that enalapril may play a positive role in lipid metabolism (**Fig. S6A**). Accordingly, we analyzed serum lipid levels in enalapril-treated mice. Typically, aging leads to a decline in lipid metabolism in the serum, causing an accumulation of triglycerides (TGs) and low-density lipoprotein (LDL) and a decrease in high-density lipoprotein (HDL), contributing to oxidative stress and conditions such as hyperlipidemia and fatty liver(A. A. Johnson & Stolzing, 2019). Following enalapril treatment, the mice presented significant

505 reductions in TG and LDL levels and a noticeable increase in HDL levels (**Fig. 6K–M**).
506 These results suggest that enalapril has the potential to increase lipid metabolism in
507 aged mice, thereby mitigating the increase in blood lipid levels.

508 To evaluate the improvements in the aging process induced by enalapril in various
509 organ systems, we conducted pathological examinations of mouse tissues. A decrease
510 in β-gal staining was observed in the brain, liver and spleen of enalapril-treated mice,
511 suggesting an alleviation of aging-associated phenotypes (**Fig. 6N, Fig. S9A–C**). Given
512 the effects of enalapril on brain function, we further examined pathological markers in
513 the brain. Periodic acid-Schiff (PAS) staining, which is indicative of glycogen
514 deposition, revealed a significant reduction in glycogen near the hippocampus (**Fig. 6O,**
515 **Fig. S9D**). Congo red staining, which detects amyloid protein deposition, also revealed
516 reduced staining in the cerebral cortex (**Fig. 6P, Fig. S9E**). In the kidney, sirius red
517 staining, which highlights abnormal collagen fibers or fibrosis, revealed significant red
518 staining around blood vessels in control mice. However, this staining was noticeably
519 reduced in the kidneys of the mice treated with enalapril (**Fig. 6Q, Fig. S9F**). These
520 findings suggest that enalapril has a beneficial effect on fibrosis in the kidneys of aged
521 mice, which aligns with the observed improvement in plasma creatinine levels (**Fig. 6I**).
522 Furthermore, analysis of spleen, kidney and liver sections from enalapril-treated mice
523 revealed a reduction in Oil Red O staining, with the kidneys and liver showing the most
524 significant changes (**Fig. 6R, Fig. S9G–I**). This finding aligned with the consistent
525 decrease in lipid-related molecular content in plasma, indicating that enalapril has a role
526 in reducing age-related lipid accumulation (**Fig. 6K–M**). Hematoxylin and eosin (H&E)
527 staining of the liver revealed a decrease in cavities and increased tissue density in mice
528 treated with enalapril, suggesting its role in enhancing liver cell proliferation and
529 regeneration (**Fig. 6S, Fig. S9J**).

530 In summary, enalapril significantly mitigated multiple pathological markers
531 associated with aging, including lipid droplets, amyloid, glycogen deposition, and
532 fibrosis, in the brain, kidneys, liver, heart and spleen of aged mice. These
533 comprehensive improvements contribute to an overall amelioration of their aging status.

DISCUSSION

Since the early 2000s, the National Institutes of Health (NIH) has been pioneering the Interventions Testing Program (ITP), an initiative aimed at harnessing existing drugs or small molecules to decelerate the aging process(Harrison et al., 2009; Nadon et al., 2008; Strong et al., 2016). This approach repurposes established medications for novel uses, maximizing the potential of known compounds. It has accelerated the transition of anti-aging therapies from discovery to clinical application, ensures their safety and bolsters a comprehensive anti-aging drug screening strategy.

In our study, we discovered that enalapril, a commonly prescribed ACE inhibitor for hypertension, has significant anti-senescence effects at both the cellular and organismal levels (**Fig. 7**). Enalapril demonstrated a notable ability to attenuate aging-related physiological decline across multiple organs, including the brain, kidneys, and liver. This finding suggests its potential to reduce the risk of disease across multiple organs, slow the overall aging process and extend both the healthspan and lifespan of mice. This observation aligns with previous reports on the lifespan-extending effects of other ACE inhibitors, such as captopril, which have been shown to increase longevity in organisms such as *C. elegans* and mice(Egan et al., 2024; Kumar, Dietrich, & Kornfeld, 2016; Strong et al., 2022). However, our screening process revealed that enalapril outperformed captopril and other antihypertensive drugs in ameliorating senescent phenotypes, although captopril and other antihypertensive drugs also exhibited the ability to delay senescence. These findings indicate that enalapril may have unique or more potent mechanisms of action that contribute to its anti-senescence effects, warranting further mechanistic studies to better understand its molecular targets.

Mechanistically, our data revealed that enalapril enhances the phosphorylation of Smad1/5/9, a critical signaling pathway that regulates various cellular processes, including cell proliferation and the oxidative stress response. Phosphorylation of Smad1/5/9 facilitates its nuclear translocation, where it acts as a transcriptional regulator to upregulate downstream genes, such as those involved in cell cycle regulation and antioxidative responses. These findings suggest that the ability of enalapril to modulate the pSmad1/5/9 pathway contributes to its protective effects

against oxidative stress, a well-established hallmark of aging. By reducing ROS levels and promoting cell proliferation, enalapril effectively delays the progression of cellular senescence and reduces organismal aging-related phenotypes. This finding not only highlights the potential of phosphorylated Smad1/5/9 as a therapeutic target for anti-senescence interventions but also reveals a novel antioxidative mechanism of enalapril action.

Several FDA-approved drugs have been repurposed for anti-aging applications, demonstrating a wide range of mechanisms and effects. These include rapamycin, metformin, and NAD^+ precursors. For example, rapamycin, which was originally used as an immunosuppressant to prevent organ transplant rejection, inhibits the mTOR pathway, which is associated with cell growth and metabolism(S. C. Johnson, Rabinovitch, & Kaeberlein, 2013). It extends the lifespan of mice and shows potential anti-aging effects across various species(Harrison et al., 2009). Compared with other repurposed anti-aging drugs, enalapril offers distinct advantages because of its unique mechanism of action. As an ACE inhibitor, enalapril inherently targets the renin–angiotensin system, providing vascular protection(Schmieder, Hilgers, Schlaich, & Schmidt, 2007; Yamamoto & Rakugi, 2021). Compared with repurposed drugs such as rapamycin, which may have more pronounced side effects, such as immunosuppression, limiting their long-term use, enalapril has a well-established safety profile(Janes & Fruman, 2009; Saunders, Metcalfe, & Nicholson, 2001). This can facilitate faster clinical translation for anti-aging applications. Moreover, our study revealed that enalapril reduces ROS through the pSmad1/5/9-antioxidant axis, highlighting its potential for antioxidation, a hallmark of aging that is less directly targeted by drugs such as rapamycin or metformin. Additionally, enalapril enhances multi-organ function, particularly in the brain, kidneys, and liver. Its well-established safety profile further supports enalapril as a promising candidate for clinical anti-aging applications, with the potential to complement existing therapies by promoting both vascular health and systemic antioxidative and anti-inflammatory effects.

Aging is a highly complex and multifactorial process(Campisi, 2013; Jazwinski, 1996). It involves intricate interactions among various signaling pathways and crosstalk

between tissues and organs, especially during individual aging(Jazwinski, 1996; Munoz-Espin & Serrano, 2014). Notably, enalapril is not uniform across all organs and tissues, as indicated by the differential improvement in aging phenotypes among various tissues. For example, enalapril significantly improved the physiological functions of the brain, muscle and other organs, but the specific pathways and mechanisms by which these effects are mediated might differ among organs. This observation suggests that the tissue-specific effects of enalapril may be mediated by differential activation of signaling pathways, including those beyond the Smad1/5/9 axis, which are known to play crucial roles in aging. Future studies should focus on delineating these tissue-specific mechanisms to fully understand the scope of the anti-aging effects of enalapril. Moreover, improvements in metabolic function in the liver could have downstream effects on brain function, as metabolic dysregulation is known to exacerbate neurodegenerative diseases. Similarly, enhanced vascular health resulting from the antihypertensive properties of enalapril may contribute to improved brain perfusion, reducing the risk of age-related cognitive decline. Therefore, exploring the systemic effects of enalapril and how improvements in one organ system may benefit others should be a priority for future research. Furthermore, given the established role of enalapril as an antihypertensive drug, assessing its potential side effects when it is repurposed for anti-aging purposes is essential. Identifying strategies to minimize these side effects while optimizing their anti-aging effects is an important area of investigation. In conclusion, our study identified enalapril as a promising candidate for repurposing as an anti-senescence drug with antioxidative and promoting effects on cell proliferation. These findings open avenues for the development of targeted therapies aimed at mitigating aging and promoting healthy longevity in clinical settings, providing a foundation for guiding future research in the realm of anti-aging drug interventions.

DATA AVAILABILITY

All related sequencing data have been uploaded to the NCBI Gene Expression Omnibus and are accessible through accession numbers GSE277861 and GSE277862.

ACKNOWLEDGMENTS

We thank Dr. Xuehui Lyu (Peking University) and Shuo Chen (Center for Excellence in Molecular Cell Science, Chinese Academy of Sciences) for suggestions regarding data organization. We thank the National Center for Protein Sciences at Peking University for assisting with the cDNA library and the Core Facilities of Life Sciences, Peking University, for assisting with the confocal microscopy. We are also grateful to the Behavioral Platform of the Animal Center at Peking University for assisting with the behavioral experiments involving the mice.

AUTHOR CONTRIBUTIONS

W.T. oversaw the study and obtained financial support. W.C.L. conducted the main bench experiments. H.C.W. analyzed the data. Z.H.D. and J.N.H. helped prepare the mice samples. R.W., F.J.M. and J.L.B. helped analyze the data. L.J.Z. helped guide the experiment. W.C.L., Y. T. G. and C. Z. prepared the original manuscripts. All the authors read and approved the final version.

FUNDING

This work was supported by the National Key Research and Development Program of China (2021YFA0909300).

COMPETING INTEREST DECLARATION

The authors have no conflicts of interest to declare.

SUPPLEMENTAL INFORMATION

Additional supplementary information includes supplementary figures and tables in the attachment.

REFERENCES

Baker, D. J., Wijshake, T., Tchkonia, T., LeBrasseur, N. K., Childs, B. G., van de Sluis, B., . . . van Deursen, J. M. (2011). Clearance of p16Ink4a-positive senescent cells delays ageing-associated disorders. *Nature, 479*(7372), 232-236. doi:10.1038/nature10600

Bharath, L. P., Agrawal, M., McCambridge, G., Nicholas, D. A., Hasturk, H., Liu, J., . . . Nikolajczyk, B. S. (2020). Metformin Enhances Autophagy and Normalizes Mitochondrial Function to Alleviate Aging-Associated Inflammation. *Cell Metab, 32*(1), 44-55 e46. doi:10.1016/j.cmet.2020.04.015

Campisi, J. (2013). Aging, cellular senescence, and cancer. *Annu Rev Physiol, 75*, 685-705. doi:10.1146/annurev-physiol-030212-183653

Childs, B. G., Gluscevic, M., Baker, D. J., Laberge, R. M., Marquess, D., Dananberg, J., & van Deursen, J. M. (2017). Senescent cells: an emerging target for diseases of ageing. *Nat Rev Drug Discov, 16*(10), 718-735. doi:10.1038/nrd.2017.116

Cohen, A. A., Ferrucci, L., Fülöp, T., Gravel, D., Hao, N., Kriete, A., . . . Varadhan, R. (2022). A complex systems approach to aging biology. *Nature Aging, 2*(7), 580-591. doi:10.1038/s43587-022-00252-6

Coppe, J. P., Patil, C. K., Rodier, F., Sun, Y., Munoz, D. P., Goldstein, J., . . . Campisi, J. (2008). Senescence-associated secretory phenotypes reveal cell-nonautonomous functions of oncogenic RAS and the p53 tumor suppressor. *PLoS Biol, 6*(12), 2853-2868. doi:10.1371/journal.pbio.0060301

Dimri, G. P., Lee, X., Basile, G., Acosta, M., Scott, G., Roskelley, C., . . . et al. (1995). A biomarker that identifies senescent human cells in culture and in aging skin in vivo. *Proc Natl Acad Sci U S A, 92*(20), 9363-9367. doi:10.1073/pnas.92.20.9363

Egan, B. M., Pohl, F., Anderson, X., Williams, S. C., Gregory Adodo, I., Hunt, P., . . . Kornfeld, K. (2024). The ACE inhibitor captopril inhibits ACN-1 to control dauer formation and aging. *Development, 151*(3). doi:10.1242/dev.202146

Fei, M. Y., Wang, Y., Chang, B. H., Xue, K., Dong, F. Y., Huang, D., . . . Wang, L. (2023). The non-cell-autonomous function of ID1 promotes AML progression via ANGPTL7 from the microenvironment. *Blood, 142*(10), 903-917. doi:10.1182/blood.2022019537

Genander, M., Cook, P. J., Ramsköld, D., Keyes, B. E., Mertz, A. F., Sandberg, R., & Fuchs, E. (2014). BMP Signaling and Its pSMAD1/5 Target Genes Differentially Regulate Hair Follicle Stem Cell Lineages. *Cell Stem Cell, 15*(5), 619-633. doi:10.1016/j.stem.2014.09.009

Gu, Z. (2022). Complex heatmap visualization. *Imeta, 1*(3), e43. doi:10.1002/imt2.43

Guglielmi, L., Heliot, C., Kumar, S., Alexandrov, Y., Gori, I., Papaleonidopoulou, F., . . . Hill, C. S. (2021). Smad4 controls signaling robustness and morphogenesis by differentially contributing to the Nodal and BMP pathways. *Nature Communications, 12*(1). doi:ARTN

6374 10.1038/s41467-021-26486-3

Harrison, D. E., Strong, R., Allison, D. B., Ames, B. N., Astle, C. M., Atamna, H., . . . Miller, R. A. (2014). Acarbose, 17-α-estradiol, and nordihydroguaiaretic acid extend mouse lifespan preferentially in males. *Aging Cell, 13*(2), 273-282. doi:10.1111/acel.12170

Harrison, D. E., Strong, R., Sharp, Z. D., Nelson, J. F., Astle, C. M., Flurkey, K., . . . Miller, R. A. (2009). Rapamycin fed late in life extends lifespan in genetically heterogeneous mice. *Nature, 460*(7253), 392-U108. doi:10.1038/nature08221

Hayashi, Y., Hsiao, E. C., Sami, S., Lancero, M., Schlieve, C. R., Nguyen, T., . . . Yamanaka, S. (2016). BMP-SMAD-ID promotes reprogramming to pluripotency by inhibiting p16/INK4A-dependent senescence. *Proc Natl Acad Sci U S A, 113*(46), 13057-13062. doi:10.1073/pnas.1603668113

Janes, M. R., & Fruman, D. A. (2009). Immune Regulation by Rapamycin: Moving Beyond T Cells. *Science Signaling, 2*(67). doi:ARTN pe25 10.1126/scisignal.267pe25

Jazwinski, S. M. (1996). Longevity, genes, and aging. *Science, 273*(5271), 54-59. doi:10.1126/science.273.5271.54

Johnson, A. A., & Stolzing, A. (2019). The role of lipid metabolism in aging, lifespan regulation, and age-related disease. *Aging Cell, 18*(6). doi:ARTN e13048 10.1111/acel.13048

Johnson, S. C., Rabinovitch, P. S., & Kaeberlein, M. (2013). mTOR is a key modulator of ageing and age-related disease. *Nature, 493*(7432), 338-345. doi:10.1038/nature11861

Khosla, S., Farr, J. N., Tchkonia, T., & Kirkland, J. L. (2020). The role of cellular senescence in ageing and endocrine disease. *Nat Rev Endocrinol, 16*(5), 263-275. doi:10.1038/s41574-020-0335-y

Kim, D., Paggi, J. M., Park, C., Bennett, C., & Salzberg, S. L. (2019). Graph-based genome alignment and genotyping with HISAT2 and HISAT-genotype. *Nat Biotechnol, 37*(8), 907-915. doi:10.1038/s41587-019-0201-4

Kirkland, J. L. (2016). Translating the Science of Aging into Therapeutic Interventions. *Cold Spring Harb Perspect Med, 6*(3), a025908. doi:10.1101/cshperspect.a025908

Kumar, S., Dietrich, N., & Kornfeld, K. (2016). Angiotensin Converting Enzyme (ACE) Inhibitor Extends Caenorhabditis elegans Life Span. *PLoS Genet, 12*(2), e1005866. doi:10.1371/journal.pgen.1005866

Langmead, B., & Salzberg, S. L. (2012). Fast gapped-read alignment with Bowtie 2. *Nat Methods, 9*(4), 357-359. doi:10.1038/nmeth.1923

Li, H., Handsaker, B., Wysoker, A., Fennell, T., Ruan, J., Homer, N., . . . Genome Project Data Processing, S. (2009). The Sequence Alignment/Map format and SAMtools. *Bioinformatics, 25*(16), 2078-2079. doi:10.1093/bioinformatics/btp352

Liang, Y. Y., Brunicardi, F. C., & Lin, X. (2009). Smad3 mediates immediate early induction of Id1 by TGF-beta. *Cell Res, 19*(1), 140-148. doi:10.1038/cr.2008.321

Liao, Y., Smyth, G. K., & Shi, W. (2014). featureCounts: an efficient general purpose program for assigning sequence reads to genomic features. *Bioinformatics, 30*(7), 923-930. doi:10.1093/bioinformatics/btt656

Lihua, Z., Claude, G., & Nathan, L. (2010). ChIPpeakAnno: a Bioconductor package to annotate ChIP-seq and ChIP-chip data. *BMC Bioinformatics, 11*, 237.

Lopez-Otin, C., Blasco, M. A., Partridge, L., Serrano, M., & Kroemer, G. (2023). Hallmarks of aging: An expanding universe. *Cell, 186*(2), 243-278. doi:10.1016/j.cell.2022.11.001

Love, M. I., Huber, W., & Anders, S. (2014). Moderated estimation of fold change and dispersion for RNA-seq data with DESeq2. *Genome Biol, 15*(12), 550. doi:10.1186/s13059-014-0550-8

Lyden, D., Young, A. Z., Zagzag, D., Yan, W., Gerald, W., O'Reilly, R., . . . Benezra, R. (1999). Id1 and Id3 are required for neurogenesis, angiogenesis and vascularization of tumour xenografts. *Nature, 401*(6754), 670-677. doi:10.1038/44334

Lyu, G. L., Guan, Y. T., Zhang, C., Zong, L., Sun, L., Huang, X. K., . . . Tao, W. (2018). TGF-β signaling alters H4K20me3 status via miR-29 and contributes to cellular senescence and cardiac aging (vol 9, 2560, 2018). *Nature Communications, 9*. doi:ARTN 4134 10.1038/s41467-018-06710-3

Miyazono, K., Maeda, S., & Imamura, T. (2005). BMP receptor signaling: Transcriptional targets, regulation of signals, and signaling cross-talk. *Cytokine & Growth Factor Reviews, 16*(3), 251-263. doi:10.1016/j.cytogfr.2005.01.009

Munoz-Espin, D., & Serrano, M. (2014). Cellular senescence: from physiology to pathology. *Nat Rev Mol Cell Biol, 15*(7), 482-496. doi:10.1038/nrm3823

Nadon, N. L., Strong, R., Miller, R. A., Nelson, J., Javors, M., Sharp, Z. D., . . . Harrison, D. E. (2008). Design of aging intervention studies: the NIA interventions testing program. *Age, 30*(4), 187-199. doi:10.1007/s11357-008-9048-1

Orlowski, J. (2017). SMAD5 signaling: more than meets the nuclei. *Cell Res, 27*(9), 1075-1076. doi:10.1038/cr.2017.101

Radulescu, C. I., Cerar, V., Haslehurst, P., Kopanitsa, M., & Barnes, S. J. (2021). The aging mouse brain: cognition, connectivity and calcium. *Cell Calcium, 94*, 102358. doi:10.1016/j.ceca.2021.102358

Rahman, M. S., Akhtar, N., Jamil, H. M., Banik, R. S., & Asaduzzaman, S. M. (2015). TGF-β/BMP signaling and other molecular events: regulation of osteoblastogenesis and bone formation. *Bone Research, 3*. doi:ARTN 15005 10.1038/boneres.2015.5

Ramachandran, A., Vizán, P., Das, D., Chakravarty, P., Vogt, J., Rogers, K. W., . . . Hill, C. S. (2018). TGF-β uses a novel mode of receptor activation to phosphorylate SMAD1/5 and induce epithelial-to-mesenchymal transition. *Elife, 7*. doi:ARTN e31756 10.7554/eLife.31756

Ramirez, F., Dundar, F., Diehl, S., Gruning, B. A., & Manke, T. (2014). deepTools: a flexible

platform for exploring deep-sequencing data. *Nucleic Acids Res, 42*(Web Server issue), W187-191. doi:10.1093/nar/gku365

Saunders, R. N., Metcalfe, M. S., & Nicholson, M. L. (2001). Rapamycin in transplantation: A review of the evidence. *Kidney International, 59*(1), 3-16. doi:DOI 10.1046/j.1523-1755.2001.00460.x

Schmieder, R. E., Hilgers, K. F., Schlaich, M. P., & Schmidt, B. M. W. (2007). Renin-angiotensin system and cardiovascular risk. *Lancet, 369*(9568), 1208-1219. doi:10.1016/S0140-6736(07)60242-6

Senft, A. D., Bikoff, E. K., Robertson, E. J., & Costello, I. (2019). Genetic dissection of Nodal and Bmp signalling requirements during primordial germ cell development in mouse. *Nature Communications, 10*. doi:ARTN 1089 10.1038/s41467-019-09052-w

Shah, P. P., Donahue, G., Otte, G. L., Capell, B. C., Nelson, D. M., Cao, K., . . . Berger, S. L. (2013). Lamin B1 depletion in senescent cells triggers large-scale changes in gene expression and the chromatin landscape. *Genes Dev, 27*(16), 1787-1799. doi:10.1101/gad.223834.113

Strong, R., Miller, R. A., Antebi, A., Astle, C. M., Bogue, M., Denzel, M. S., . . . Harrison, D. E. (2016). Longer lifespan in male mice treated with a weakly estrogenic agonist, an antioxidant, an -glucosidase inhibitor or a Nrf2-inducer. *Aging Cell, 15*(5), 872-884. doi:10.1111/acel.12496

Strong, R., Miller, R. A., Cheng, C. J., Nelson, J. F., Gelfond, J., Allani, S. K., . . . Harrison, D. E. (2022). Lifespan benefits for the combination of rapamycin plus acarbose and for captopril in genetically heterogeneous mice. *Aging Cell, 21*(12). doi:10.1111/acel.13724

Sun, Y., Yan, K., Wang, Y., Xu, C., Wang, D., Zhou, W., . . . Xi, Q. R. (2022). Context-dependent tumor-suppressive BMP signaling in diffuse intrinsic pontine glioma regulates stemness through epigenetic regulation of CXXC5. *Nature Cancer, 3*(9), 1105-+. doi:10.1038/s43018-022-00408-8

Urist, M. R. (1965). Bone - Formation by Autoinduction. *Science, 150*(3698), 893-+. doi:DOI 10.1126/science.150.3698.893

Wu, T., Hu, E., Xu, S., Chen, M., Guo, P., Dai, Z., . . . Yu, G. (2021). clusterProfiler 4.0: A universal enrichment tool for interpreting omics data. *Innovation (Camb), 2*(3), 100141. doi:10.1016/j.xinn.2021.100141

Xu, M., Pirtskhalava, T., Farr, J. N., Weigand, B. M., Palmer, A. K., Weivoda, M. M., . . . Kirkland, J. L. (2018). Senolytics improve physical function and increase lifespan in old age. *Nat Med, 24*(8), 1246-1256. doi:10.1038/s41591-018-0092-9

Yamamoto, K., & Rakugi, H. (2021). Angiotensin receptor-neprilysin inhibitors: Comprehensive review and implications in hypertension treatment. *Hypertension Research, 44*(10), 1239-1250. doi:10.1038/s41440-021-00706-1

Ying, Q. L., Nichols, J., Chambers, I., & Smith, A. (2003). BMP induction of Id proteins suppresses

differentiation and sustains embryonic stem cell self-renewal in collaboration with STAT3. *Cell, 115*(3), 281-292. doi:Doi 10.1016/S0092-8674(03)00847-X

Yousefzadeh, M. J., Zhu, Y., McGowan, S. J., Angelini, L., Fuhrmann-Stroissnigg, H., Xu, M., . . . Niedernhofer, L. J. (2018). Fisetin is a senotherapeutic that extends health and lifespan. *Ebiomedicine, 36*, 18-28. doi:10.1016/j.ebiom.2018.09.015

Zhang, Y., Liu, T., Meyer, C. A., Eeckhoute, J., Johnson, D. S., Bernstein, B. E., . . . Liu, X. S. (2008). Model-based analysis of ChIP-Seq (MACS). *Genome Biol, 9*(9), R137. doi:10.1186/gb-2008-9-9-r137

Zhou, Y., Zhou, B., Pache, L., Chang, M., Khodabakhshi, A. H., Tanaseichuk, O., . . . Chanda, S. K. (2019). Metascape provides a biologist-oriented resource for the analysis of systems-level datasets. *Nat Commun, 10*(1), 1523. doi:10.1038/s41467-019-09234-6

Zhu, Y., Tchkonia, T., Fuhrmann-Stroissnigg, H., Dai, H. M. M., Ling, Y. Y. Y., Stout, M. B., . . . Kirkland, J. L. (2016). Identification of a novel senolytic agent, navitoclax, targeting the Bcl-2 family of anti-apoptotic factors. *Aging Cell, 15*(3), 428-435. doi:10.1111/acel.12445

Zhu, Y., Tchkonia, T., Pirtskhalava, T., Gower, A. C., Ding, H. S., Giorgadze, N., . . . Kirkland, J. L. (2015). The Achilles' heel of senescent cells: from transcriptome to senolytic drugs. *Aging Cell, 14*(4), 644-658. doi:10.1111/acel.12344

FIGURE AND FIGURE LEGENDS

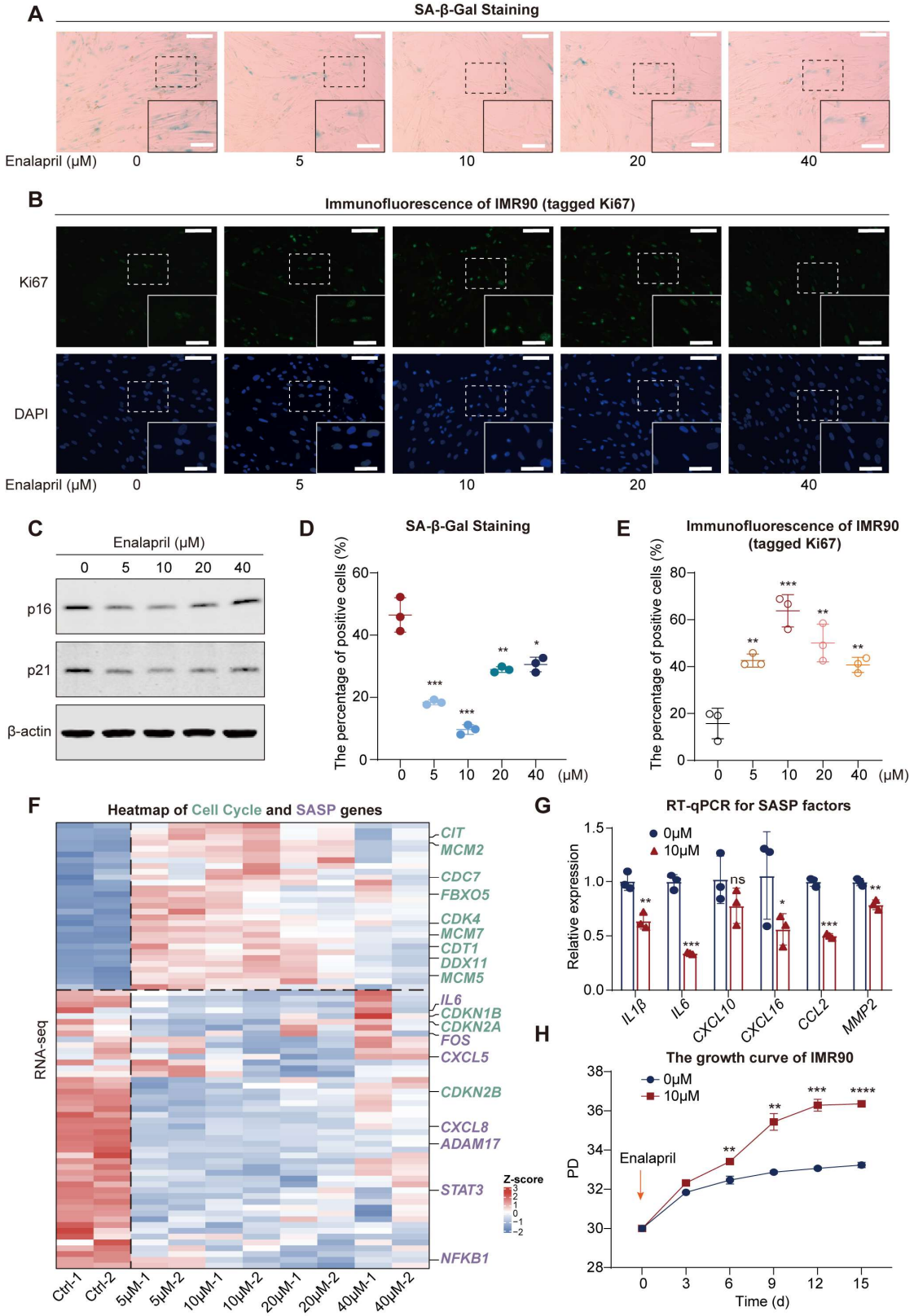

Figure 1 Enalapril alleviates cellular senescence. (**A, D**) SA-β-Gal staining (**A**) and

statistical analysis of SA-β-Gal ratios (**D**) in IMR90 cells after enalapril treatment. Scale bars, 200 μm. Enlarged scale bars, 100 μm. (**B, E**) Ki67 immunofluorescence experiment (**B**) and statistical analysis of Ki67 intensity (**E**) after enalapril treatment. Scale bars, 80 μm. Enlarged scale bars, 40 μm. (**C**) Western blot analysis showing the protein levels of p16 and p21 in IMR90 cells after enalapril treatment. (**F**) Heatmap showing cell cycle-related gene (green) upregulation and SASP gene (purple) downregulation after enalapril treatment. (**G**) RNA expression of SASP factors in IMR90 cells after enalapril treatment, with blue bars representing the control group and red bars representing the enalapril-treated group. (**H**) Growth curves of IMR90 cells after enalapril treatment. The x-axis represents the passage time, while the y-axis represents population doubling (PD). A two-tailed t test was employed; ns indicates no significant difference, *$p < 0.05$, **$p < 0.01$, ***$p < 0.001$, ****$p < 0.0001$.

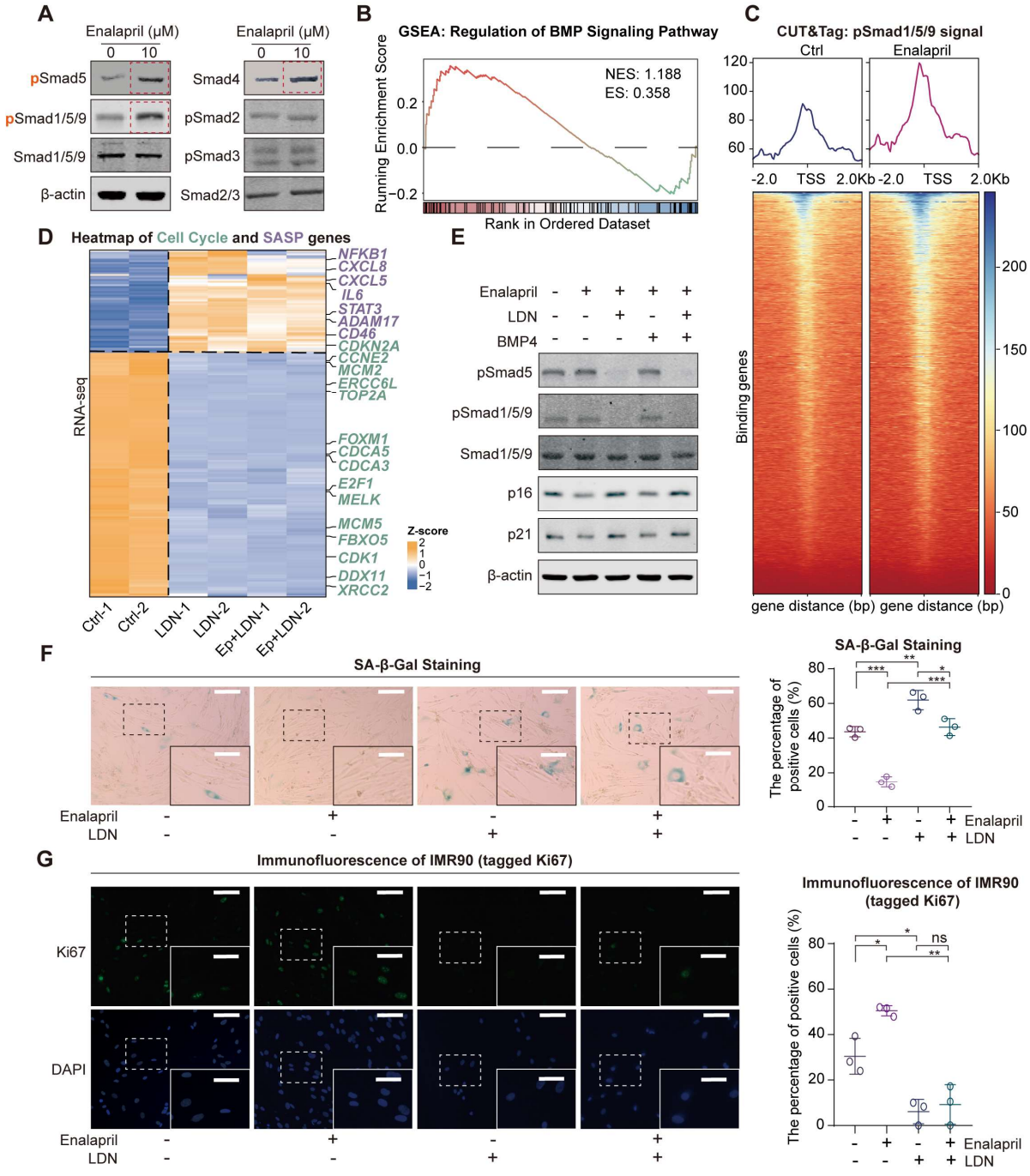

Figure 2 Phosphorylated Smad1/5/9 mediate the anti-senescence effect of enalapril. (**A**) Western blot results for the detection of pSmad5, pSmad1/5/9 and other proteins after enalapril treatment. (**B**) GSEA showing the enrichment of the BMP signaling pathway after enalapril treatment. NES, normalized enrichment score. ES, enrichment score. (**C**) Profile of pSmad1/5/9 enrichment at the TSS regions in the control group (Ctrl) and the enalapril-treated group (Enalapril). (**D**) Heatmap of cell cycle (green) and SASP-related genes (purple) in the control group (Ctrl), BMP receptor inhibitor-treated

group (LDN193189, LDN), and enalapril and BMP receptor inhibitor-cotreated group (EP+LDN). (**E**) Western blot analysis showing the protein levels of pSmad1/5/9, p16, and p21 in response to different combinations of enalapril, a BMP receptor inhibitor (LDN193189, LDN), and BMP4. (**F**) SA-β-Gal staining (left) and corresponding ratio statistical chart (right) of IMR90 cells treated with different combinations of enalapril, a BMP receptor inhibitor (LDN193189, LDN), and BMP4. Scale bars, 200 μm. Enlarged scale bars, 100 μm. (**G**) Ki67 immunofluorescence experiment (left) and intensity statistical chart (right) of IMR90 cells treated with different combinations of enalapril, a BMP receptor inhibitor (LDN193189, LDN), and BMP4. Scale bars, 80 μm. Enlarged scale bars, 40 μm. A two-tailed t test was employed; ns indicates no significant difference, $*p < 0.05$, $**p < 0.01$, $***p < 0.001$.

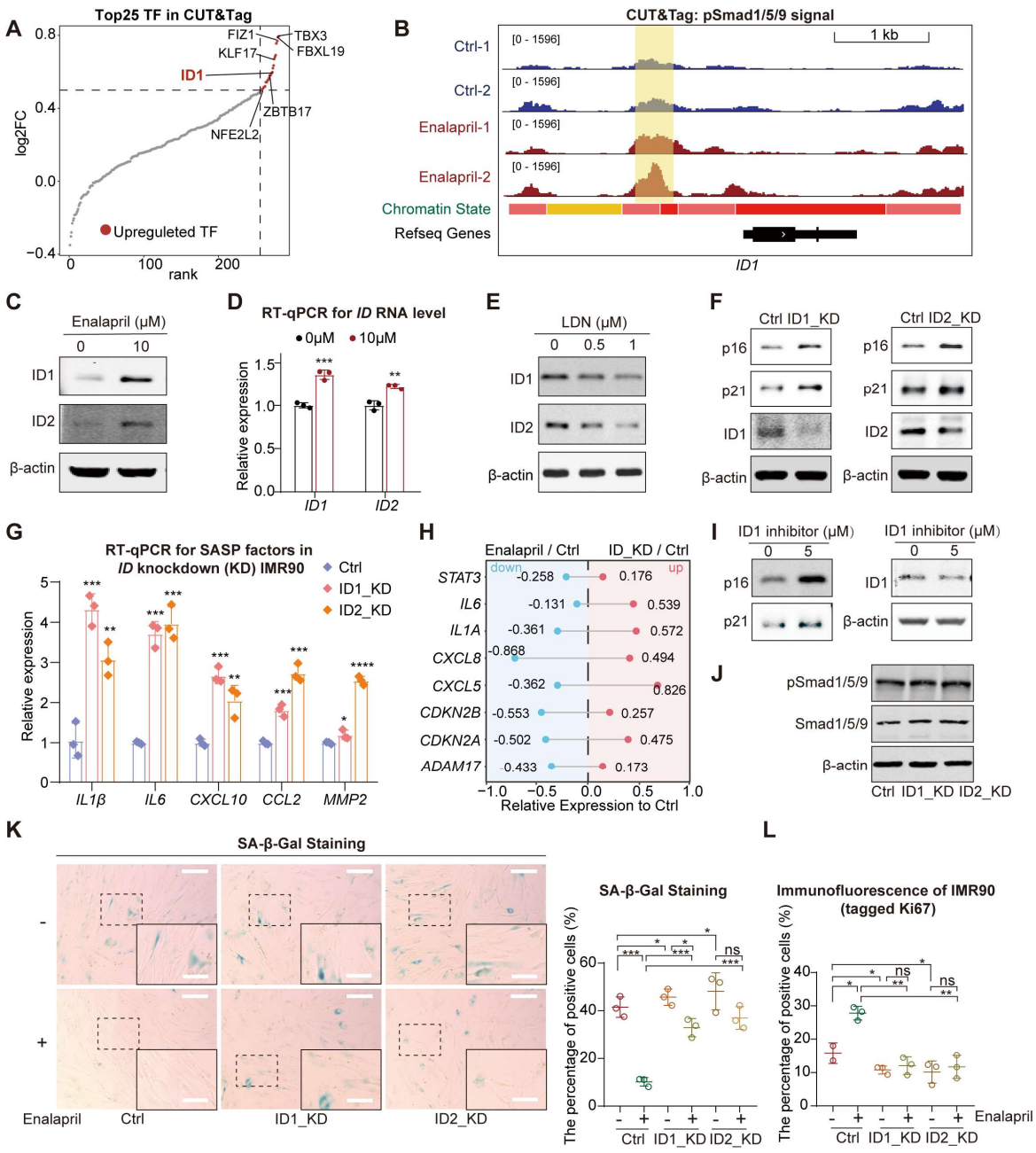

Figure 3 pSmad1/5/9 regulate ID-induced inhibition of p16, p21 and SASP. (**A**) Changes in the peaks of all transcription factors identified by CUT&Tag following enalapril treatment, with red dots indicating transcription factors with increased peak intensity (Upregulated TFs). (**B**) Integrative Genomics Viewer (IGV) showing pSmad1/5/9 signals near the *ID1* region between the control group (Ctrl) and the enalapril treatment group (Enalapril). The vertical yellow boxes indicate regions with increased signal intensity. (**C**) Western blot analysis showing the changes in the protein levels of ID1 and ID2 following enalapril treatment. (**D**) Changes in the RNA levels of ID1 and ID2 following enalapril treatment. (**E**) Western blot analysis showing the

protein levels of ID1 and ID2 following treatment with a BMP receptor inhibitor (LDN193189, LDN). (**F, I**) Western blot showing the changes in the protein levels of p16 and p21 following the knockdown of *ID1* or *ID2* (**F**) or the inhibition of ID1 (**I**). (**G**) RNA expression of SASP factors after *ID* knockdown, with pink representing *ID1* knockdown and orange representing *ID2* knockdown. (**H**) Normalized average RNA expression levels of selected SASP factors and cell cycle arrest factors after enalapril treatment and *ID* knockdown. Positive values indicate upregulation, while negative values indicate downregulation. The values represent the expression levels relative to those of the Ctrl. (**J**) Western blot analysis showing pSmad1/5/9 levels following *ID1* and *ID2* knockdown. (**K**) SA-β-Gal staining (left) and SA-β-Gal ratio quantification (right) in the control group (Ctrl) and *ID*-knockdown groups (ID1_KD, ID2_KD) with or without enalapril treatment. Scale bars, 200 μm. Enlarged scale bars, 100 μm. (L) Ki67 immunofluorescence intensity in the control group (Ctrl) and *ID* knockdown groups (ID1_KD, ID2_KD), with or without enalapril treatment. A two-tailed t test was employed, ns indicates no significant difference, $^{*}p < 0.05$, $^{**}p < 0.01$, $^{***}p < 0.001$.

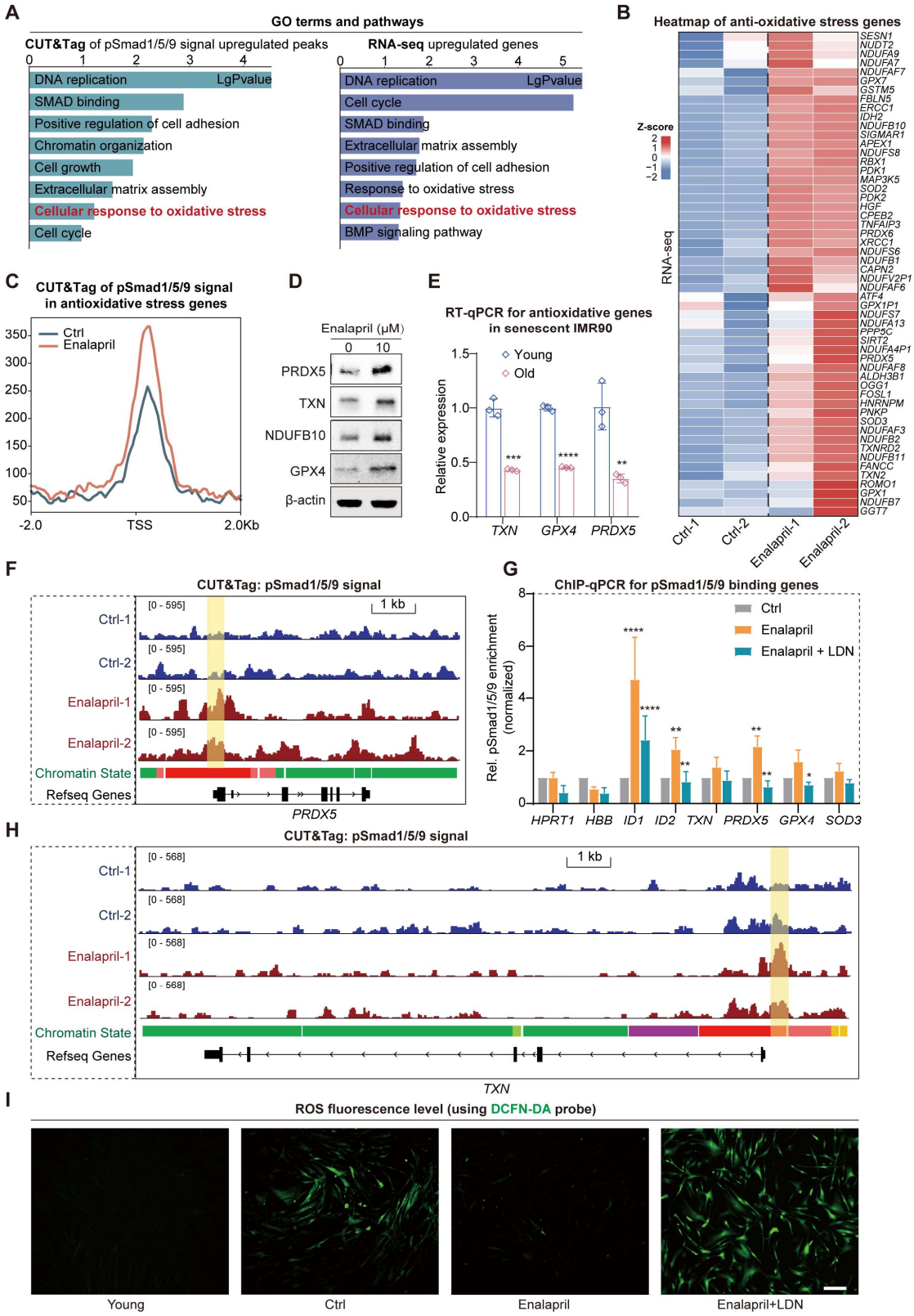

870

871 **Figure 4 pSmad1/5/9 increase the expression of antioxidative genes.** (**A**) Bar plot
872 showing the enriched GO terms and pathways associated with the CUT&Tag-
873 upregulated peaks (left) and the upregulated RNA-seq genes (right) following enalapril

treatment. (**B**) Heatmap showing the changes in the RNA expression of antioxidative genes. (**C**) Profile plot showing the increase in the pSmad1/5/9 binding signal of antioxidative genes in the TSS region following enalapril treatment. (**D**) Western blot analysis showing the protein levels of representative antioxidative genes after enalapril treatment. (**E**) Relative RNA levels of *TXN*, *GPX4*, and *PRDX5* during cellular senescence. The blue bars represent young cells, and the red bars represent senescent cells. (**F, H**) Integrative Genomics Viewer (IGV) showing pSmad1/5/9 signals near the *PRDX5* (**F**) and *TXN* (**H**) regions between the control group (Ctrl) and the enalapril treatment group (Enalapril). The vertical yellow boxes indicate regions with increased signal intensity. (**G**) ChIP-qPCR results showing pSmad1/5/9 levels at many peaks following enalapril or combination treatment with enalapril and LDN193189. The y-axis represents the normalized pSmad1/5/9 signals relative to 10% input. pSmad1/5/9 enrichment for *HPRT1* and *HBB* served as a negative control, and pSmad1/5/9 enrichment for *ID1* and *ID2* served as positive controls, as previously described. A two-tailed t test was employed, $*p < 0.05$, $**p < 0.01$, $***p < 0.001$, $****p < 0.0001$. (**I**) Detection of ROS fluorescence levels via the DCFH-DA probe in young cells, senescent cells (Ctrl), cells treated with enalapril, and cells treated with a combination of enalapril and LDN193189. Scale bars, 200 μm.

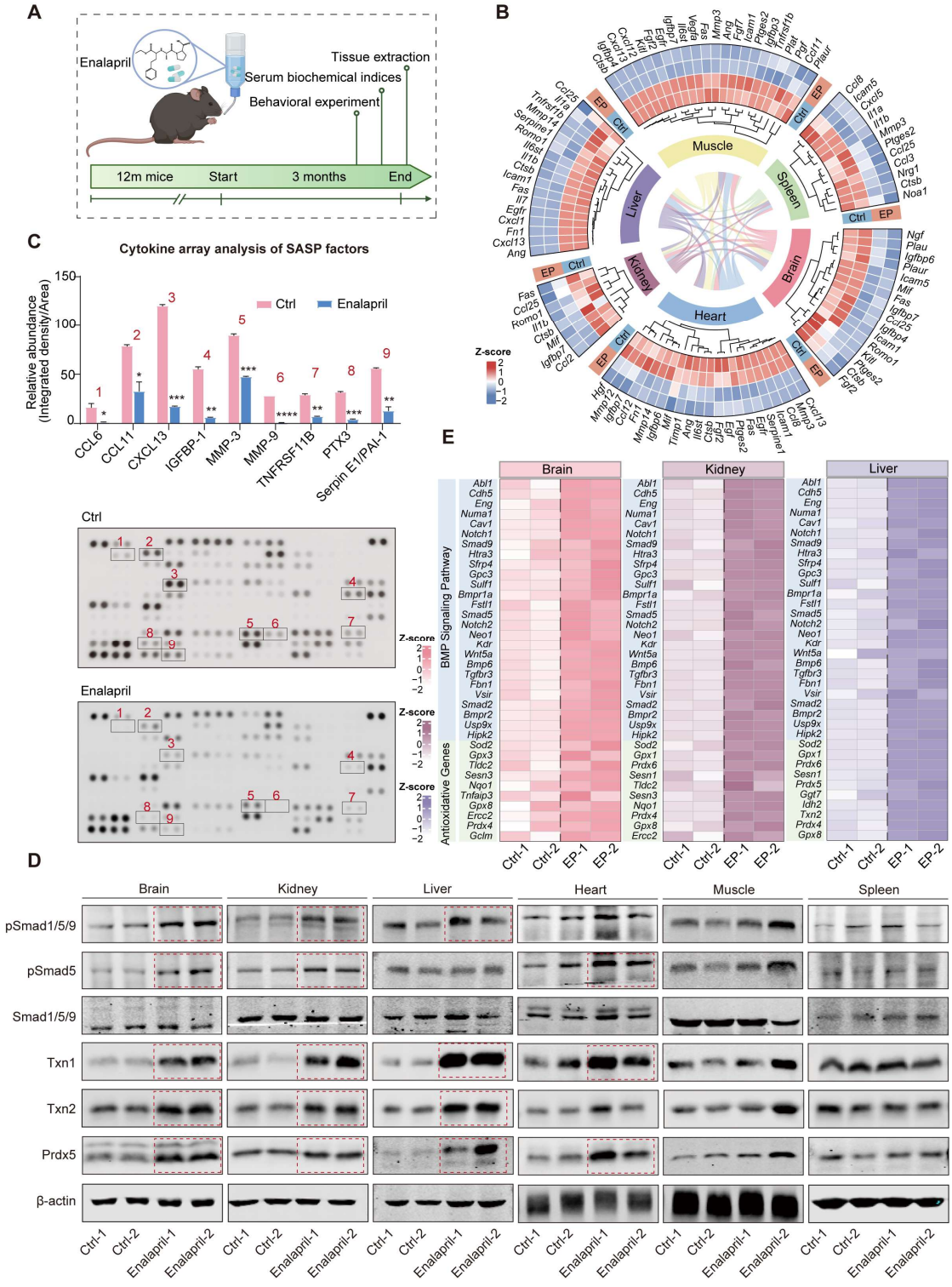

Figure 5 Enalapril exerts its anti-aging effects on mouse organs via pSmad1/5/9-antioxidative genes. (**A**) A schematic workflow of the mouse feeding and experimental procedures. Created in BioRender. Li, D. (2024) BioRender.com/u88h339 (**B**) Heatmap of RNA levels of SASP factors in various organs following enalapril treatment (EP). (**C**) Cytokine array analysis of secreted proteins (below) and relative quantitation

898 (above) of SASP factors in control serum (Ctrl) and enalapril-treated serum (Enalapril).
899 (**D**) Western blot analysis showing the protein levels of pSmad1/5/9 and antioxidative
900 genes in various organs following enalapril treatment. (**E**) Heatmap of the RNA levels
901 of BMP signaling pathway-related genes and antioxidative genes in the brain, kidney,
902 and liver following enalapril (EP) treatment.

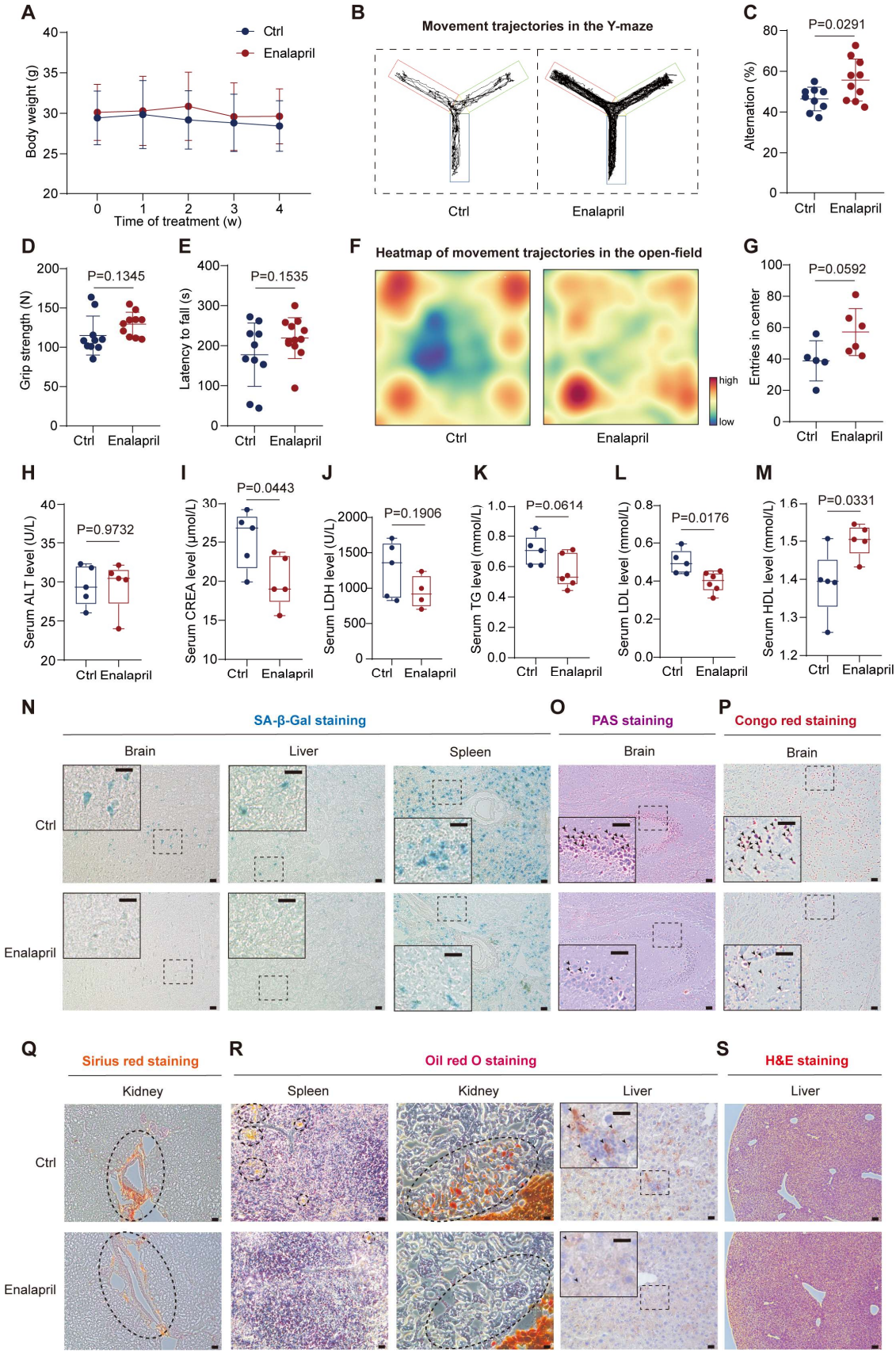

903

904 **Figure 6 Enalapril mitigates age-related degenerative changes in aged mice. (A)**

Changes in the body weights of the mice after enalapril feeding. (**B, C**) Movement trajectory (**B**) and spontaneous alternation rate (**C**) in the Y-maze of the mice after enalapril treatment. (**D, E**) Changes in the grip strength (**D**) and rotarod fall time (**E**) of the mice after enalapril treatment. (**F, G**) Heatmap of movement trajectories (**F**) and the number of entries into the central area (**G**) in the open-field test after enalapril treatment. (**H–M**) Alterations in the serum levels of aspartate transaminase (AST) (**H**), creatinine (CREA) (**I**), lactate dehydrogenase (LDH) (**J**), triglycerides (TGs) (**K**), low-density lipoprotein cholesterol (LDL) (**L**), and high-density lipoprotein cholesterol (HDL) (**M**) after enalapril treatment in mice. (**N**) SA-β-Gal staining of the brain, liver, and spleen after enalapril treatment. Scale bars, 20 μm. (**O, P**) Periodic Acid-Schiff (PAS) staining (**O**) and Congo red staining (**P**) of the brain after enalapril treatment. Scale bars, 50 μm. (**Q**) Sirius red staining of the kidney after enalapril treatment. Scale bars, 50 μm. (**R**) Oil Red O staining of the spleen, kidney and liver after enalapril treatment. Scale bars, 20 μm. (**S**) Hematoxylin and eosin (H&E) staining of the liver after enalapril treatment. Scale bars, 50 μm.

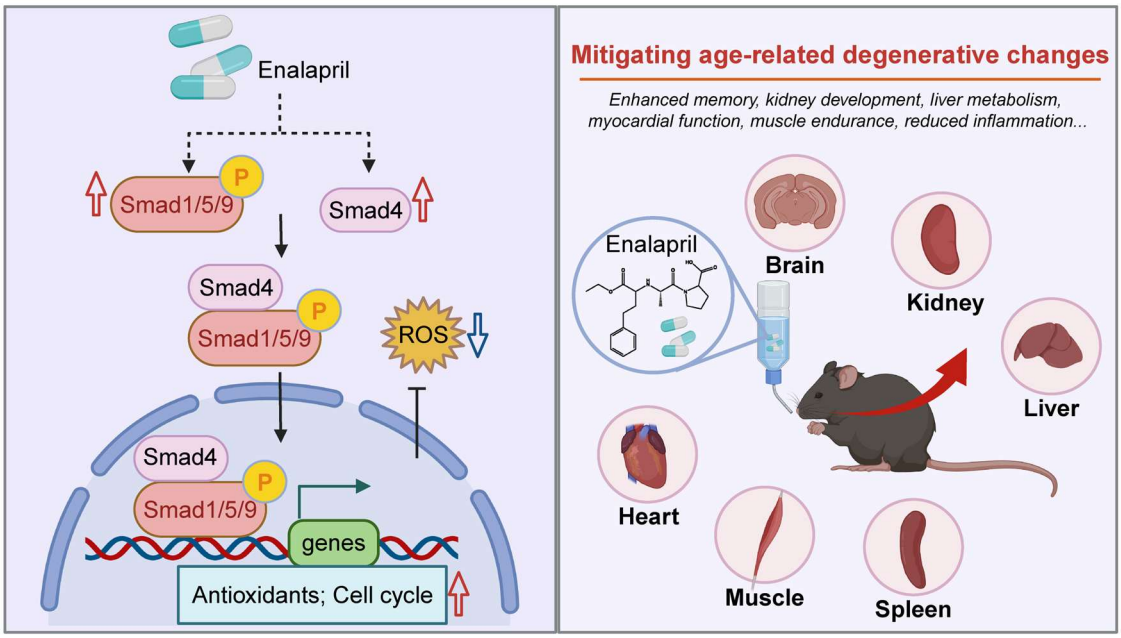

Figure 7 Summary schematic. It showing pSmad1/5/9-mediated combating cellular senescence of enalapril, and improvement of organ function in mice. Specifically, enalapril increases the level of pSmad1/5/9 and Smad4, promoting the expression of downstream genes, such as antioxidative and cell cycle related genes, thereby promoting cell proliferation and reducing ROS. Moreover, enalapril mitigates age-related degenerative changes, including enhanced memory, improved kidney function, increased liver metabolism and other organ functions. Created in BioRender. Li, D. (2024) BioRender.com/u88h339.

930 ## Supplementary Tables

931 **Table S1 Primers used in RT-qPCR**

Name	Primer sequence
IL1β	For: ATGATGGCTTATTACAGTGGCAA Rev: GTCGGAGATTCGTAGCTGGA
IL6	For: ACTCACCTCTTCAGAACGAATTG Rev: CCATCTTTGGAAGGTTCAGGTTG
CXCL10	For: GTGGCATTCAAGGAGTACCTC Rev: TGATGGCCTTCGATTCTGGATT
CXCL16	For: CCCGCCATCGGTTCAGTTC Rev: CCCCGAGTAAGCATGTCCAC
CCL2	For: AAGACCATTGTGGCCAAGGA Rev: TTCGGAGTTTGGGTTTGCT
MMP2	For: CCCACTGCGGTTTTCTCGAAT Rev: CAAAGGGGTATCCATCGCCAT
BMPR1A	For: CTTTACCACTGAAGAAGCCAGCT Rev: AGAGCTGAGTCCAGGAACCTGT
ID1	For: CTGCTCTACGACATGAACGG Rev: GAAGGTCCCTGATGTAGTCGAT
ID2	For: AGTCCCGTGAGGTCCGTTAG Rev: AGTCGTTCATGTTGTATAGCAGG
ID3	For: GAGAGGCACTCAGCTTAGCC Rev: TCCTTTTGTCGTTGGAGATGAC
ACTB	For: CACCCCGTGCTGCTGAC Rev: CCAGAGGCGTACAGGGATAG
TXN	For: GTGAAGCAGATCGAGAGCAAG Rev: CGTGGCTGAGAAGTCAACTACTA
GPX4	For: GAGGCAAGACCGAAGTAAACTAC Rev: CCGAACTGGTTACACGGGAA
PRDX5	For: CTTCACCCCTGGATGTTCCAA Rev: AGGCATCATTAACACTCAGACAG

932 **Table S2 Primers used in pSmad1/5/9 ChIP-qPCR**

Name	Primer sequence	Notes
HPRT1	For: TGTTTGGGCTATTTACTAGTTG Rev: ATAAAATGACTTAAGCCCAGAG	Negative control (Morikawa et al., 2011; Sullivan & Santos, 2020)
HBB	For: GGGCTGAGGGTTTGAAGTCC Rev: CATGGTGTCTGTTTGAGGTTGC	Negative control (Morikawa et al., 2011)
ID1	For: AGTCCGTCCGGGTTTTATG Rev: TGTGTCAGCGTCTGAACCAG	Positive control (Morikawa et al., 2011; Sullivan & Santos, 2020)
ID2	For: ACTCTATTTACCACCCCAGC Rev: AGCTTCCCTTCGTCCCCAT	
TXN	For: CAGGGCTGGATTCCTCGAAA Rev: CAAGGACGTACACACCGAGA	
PRDX5	For: GTATGGGACTAGCTGGCGTG Rev: TCACTGTACCGTCTTGCTGC	
GPX4	For: GAAGCAGAGACGGGAGGTTC Rev: CTTGTGTCTAGGAGGCCGTG	
SOD3	For: TCTGAGGGGTTAGTGGGGAG Rev: CCCCTTTCTCGTCACTCCAG	

933 **Table S3 shRNA target sequence used in knock down experiment**

Name	Target Sequence
shID1 #1	CCGGCCTACTAGTCACCAGAGACTTCTCG AGAAGTCTCTGGTGACTAGTAGGTTTTT
shID1 #2	CCGGACTCGGAATCCGAAGTTGGAACTC GAGTTCCAACTTCGGATTCCGAGTTTTTT
shID2 #1	CCGGCCCTTCTGAGTTAATGTCAAACTCG AGTTTGACATTAACTCAGAAGGGTTTTT
shID2 #2	CCGGCCCACTATTGTCAGCCTGCATCTCG AGATGCAGGCTGACAATAGTGGGTTTTT
shBMPR1A	CCGGCGCCAATCTCATACAAGCCATCTC GAGATGGCTTGTATGAGATTGGCGTTTTT

934 **Table S4 Antibodies**

Name	Source	Number
Mouse monoclonal anti-β-actin	Santa Cruz Biotechnology	Cat#sc-47778
Rabbit monoclonal anti-CDKN2A/p16INK4a	Abcam	Cat#ab108349
Rabbit monoclonal anti-p21	Abcam	Cat#ab109199
Rabbit monoclonal anti-Phospho-SMAD1 (Ser463/465)/ SMAD5 (Ser463/465)/ SMAD9 (Ser465/467)	Cell Signaling Technology	Cat#13820S
Rabbit monoclonal anti-SMAD1 + SMAD5 + SMAD9 (phosphor S463 + S465 + S467)	Abcam	Cat#ab92698
Rabbit monoclonal anti-Phospho-SMAD5 (Ser463/465)	Huabio	Cat#ET1605-5
Rabbit polyclonal anti-SMAD1/5/9	Immunoway	Cat#YT4325
Rabbit monoclonal anti-SMAD5	Huabio	Cat#ET1606-26
Rabbit monoclonal anti-SMAD4	Abcam	Cat#ab40759
Rabbit polyclonal anti-SMAD2 (Ser465/467)	Cell Signaling Technology	Cat#3101S
Rabbit monoclonal anti-SMAD3 (Ser423/425)	Cell Signaling Technology	Cat#9520S
Rabbit polyclonal anti-SMAD2/3	Cell Signaling Technology	Cat#3102S
Rabbit polyclonal anti-BMP2	Huabio	Cat#ER80602
Mouse monoclonal anti-BMP4	Huabio	Cat#EM1706-23
Rabbit polyclonal anti-ID1	Immunoway	Cat#YN0093
Rabbit polyclonal anti-ID2	Immunoway	Cat#YN2457
Rabbit polyclonal anti-PRDX5	ABclonal	Cat#A1269
Rabbit monoclonal anti-TXN	ABclonal	Cat#A4024
Rabbit monoclonal anti-TXN2	ABclonal	Cat#A4424
Rabbit polyclonal anti-NDUFB10	ABclonal	Cat#A9382
Rabbit monoclonal anti-GPX4	Abmart	Cat#T56959
IRDy 800CW Goat anti-Mouse IgG Secondary Antibody	LI-COR	Cat#926-32210
IRDy 800CW Goat anti-Rabbit IgG Secondary Antibody	LI-COR	Cat#926-32211

Supplementary Figures and legends

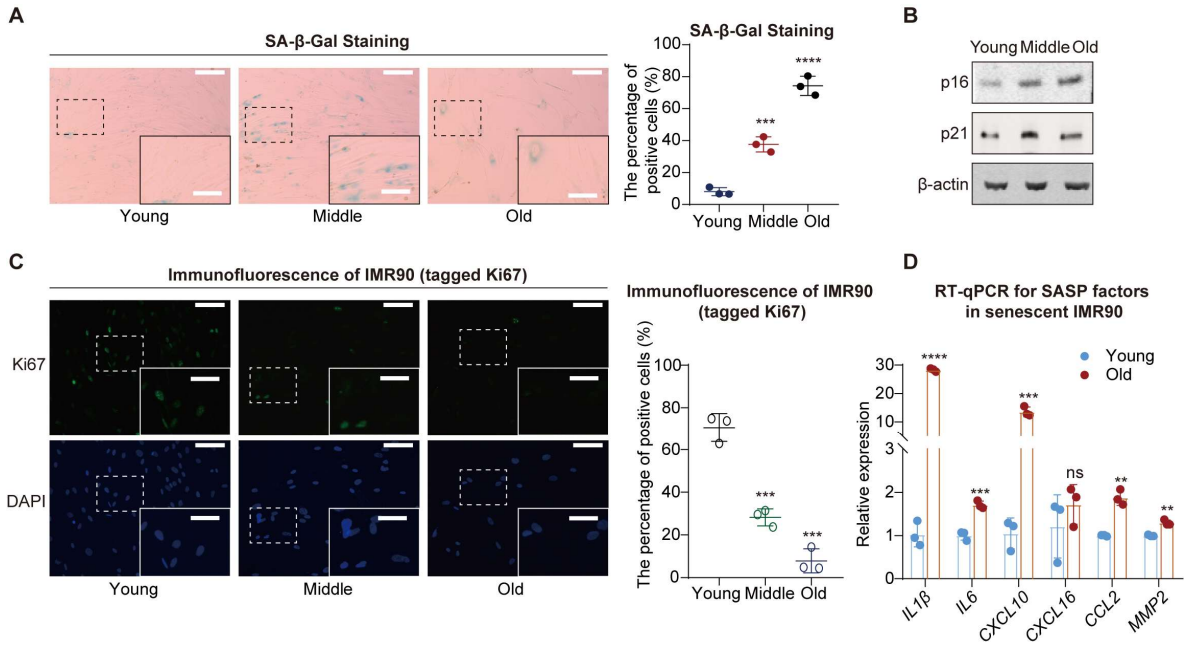

Figure S1 The expression of various senescence markers during IMR90 cell senescence. (**A**) SA-β-Gal staining (left) and statistical analysis of SA-β-Gal ratios (right) during IMR90 cell senescence. Scale bars, 200 μm. Enlarged scale bars, 100 μm. (**B**) Western blot analysis showing the protein levels of p16 and p21 in IMR90 cells at different passage. (**C**) Ki67 immunofluorescence experiment (left) and statistical analysis of Ki67 intensity (right) during IMR90 cell senescence. Scale bars, 80 μm. Enlarged scale bars, 40 μm. (**D**) RNA expression of SASP factors during IMR90 cell senescence, with blue bars representing the young group and red bars representing the old group. A two-tailed t-test was employed, ns indicates no significant difference, $^{**}p < 0.01$, $^{***}p < 0.001$, $^{****}p < 0.0001$.

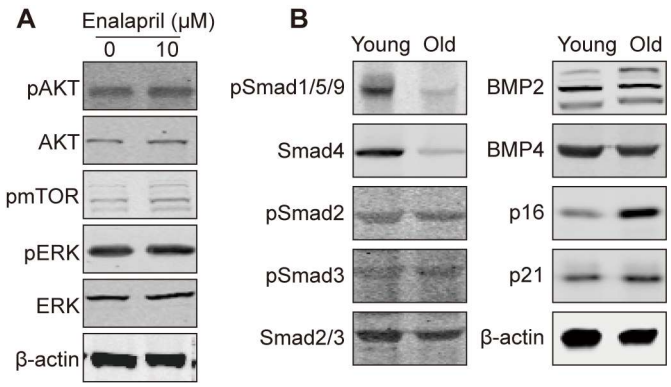

Figure S2 Alterations in critical regulators of cellular senescence. (**A**) Western blot analysis showing the changes in protein levels of key targets in classical senescence signaling pathways following enalapril treatment. (**B**) Western blot analysis showing the changes in Smad and BMP-related protein levels during IMR90 cell senescence.

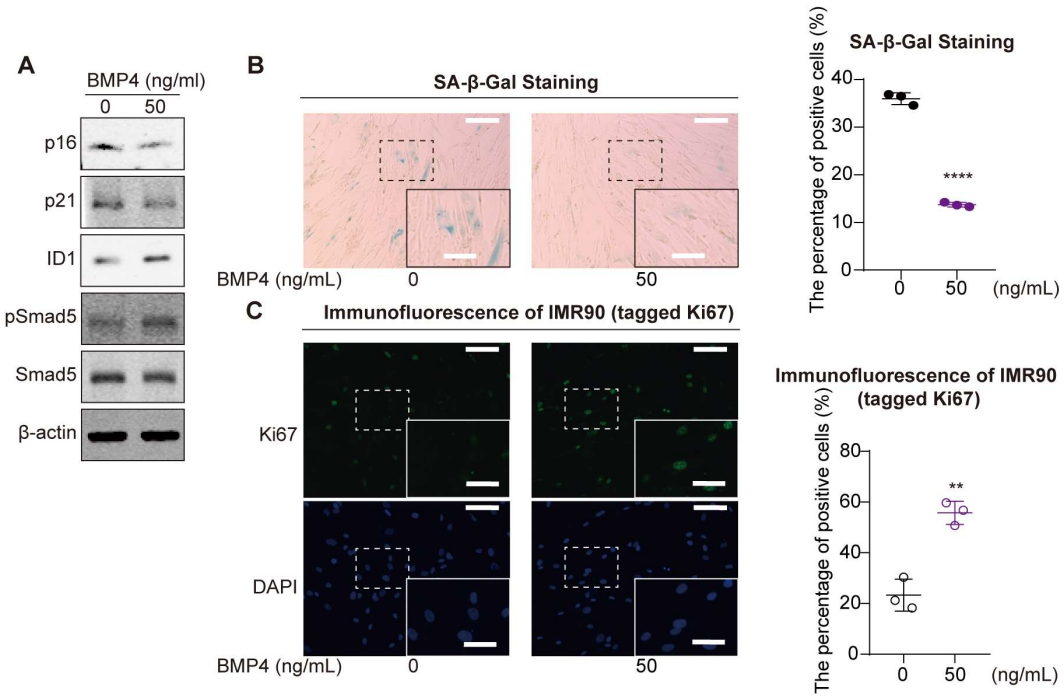

Figure S3 pSmad1/5/9 alleviates cellular senescence phenotypes. (**A**) Western blot analysis showing the changes in protein levels following BMP4 treatment. (**B**) SA-β-Gal staining (left) and corresponding ratio analysis chart (right) following BMP4 treatment. Scale bars, 200 μm. Enlarged scale bars, 100 μm. (**C**) Ki67 immunofluorescence (right) and corresponding ratio analysis chart (left) following BMP4 treatment. Scale bars, 80 μm. Enlarged scale bars, 40 μm. A two-tailed t-test was employed, $^{**}p < 0.01$, $^{****}p < 0.0001$.

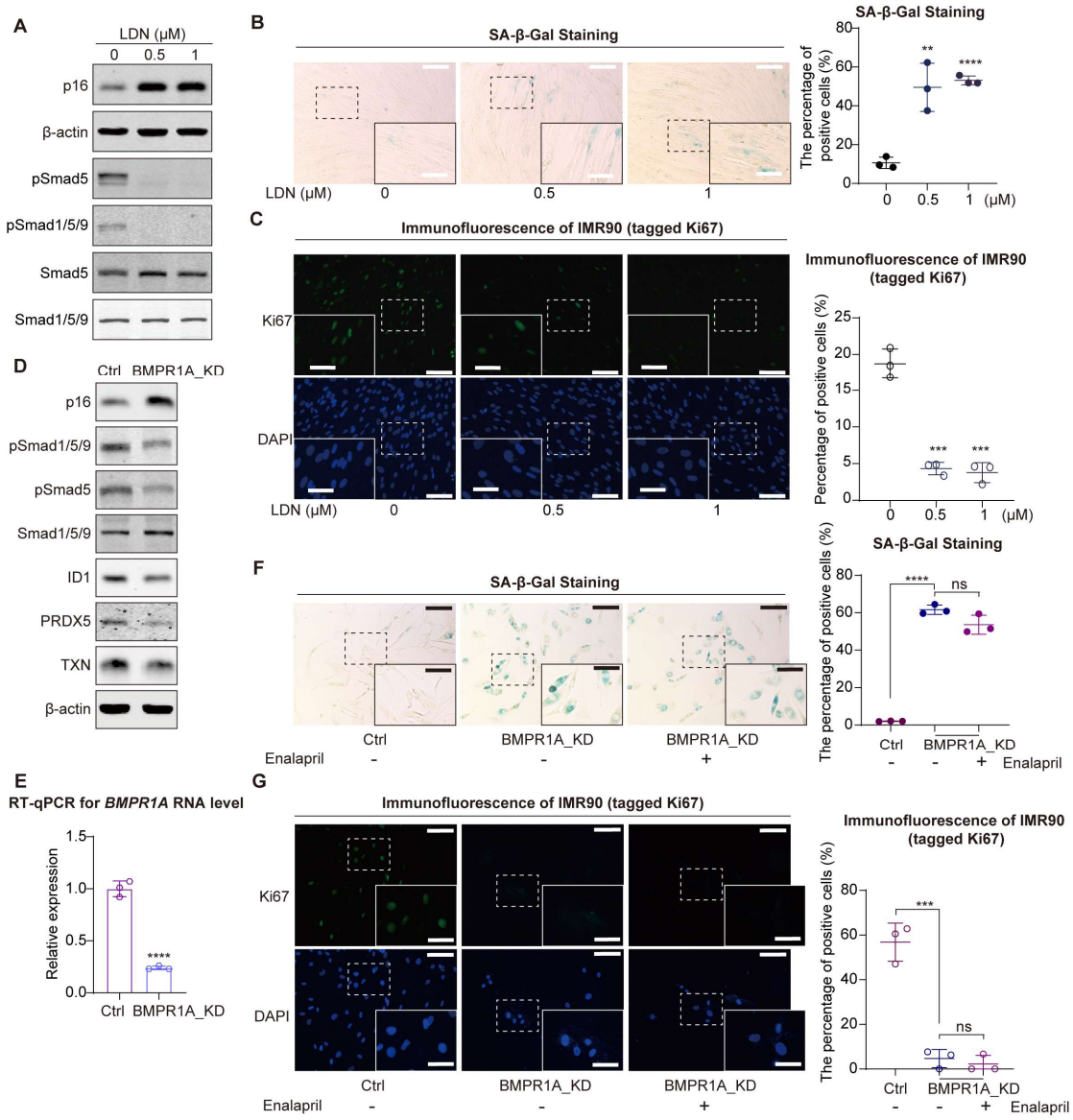

Figure S4 Reduction of pSmad1/5/9 correlates with cellular senescence. (**A**) Western blot showing the protein levels after the addition of LDN193189. (**B**) SA-β-gal staining (left) after adding LDN193189 and its corresponding staining proportion statistical chart (right). Scale bars, 200 μm. Enlarged scale bars, 100 μm. (**C**) Immunofluorescence staining for Ki67 (left) after adding LDN193189 along with the corresponding intensity statistical chart (right). Scale bars, 80 μm. Enlarged scale bars, 40 μm. (**D**) Western blot showing the protein levels following BMPR1A knockdown. (**E**) Relative RNA levels of BMPR1A following BMPR1A knockdown. (**F**) SA-β-gal staining (left) and its corresponding staining proportion statistical chart (right) in the control group (Ctrl) and *BMPR1A*-knockdown groups (BMPR1A_KD)

with enalapril treatment. Scale bars, 200 μm. Enlarged scale bars, 100 μm. (**G**) Ki67 immunofluorescence (left) and its corresponding staining proportion statistical chart (right) in the control group (Ctrl) and *BMPR1A*-knockdown groups (BMPR1A_KD) with enalapril treatment. Scale bars, 80 μm. Enlarged scale bars, 40 μm. A two-tailed t-test was employed, ns indicates no significant difference, $^{**}p < 0.01$, $^{***}p < 0.001$, $^{****}p < 0.0001$.

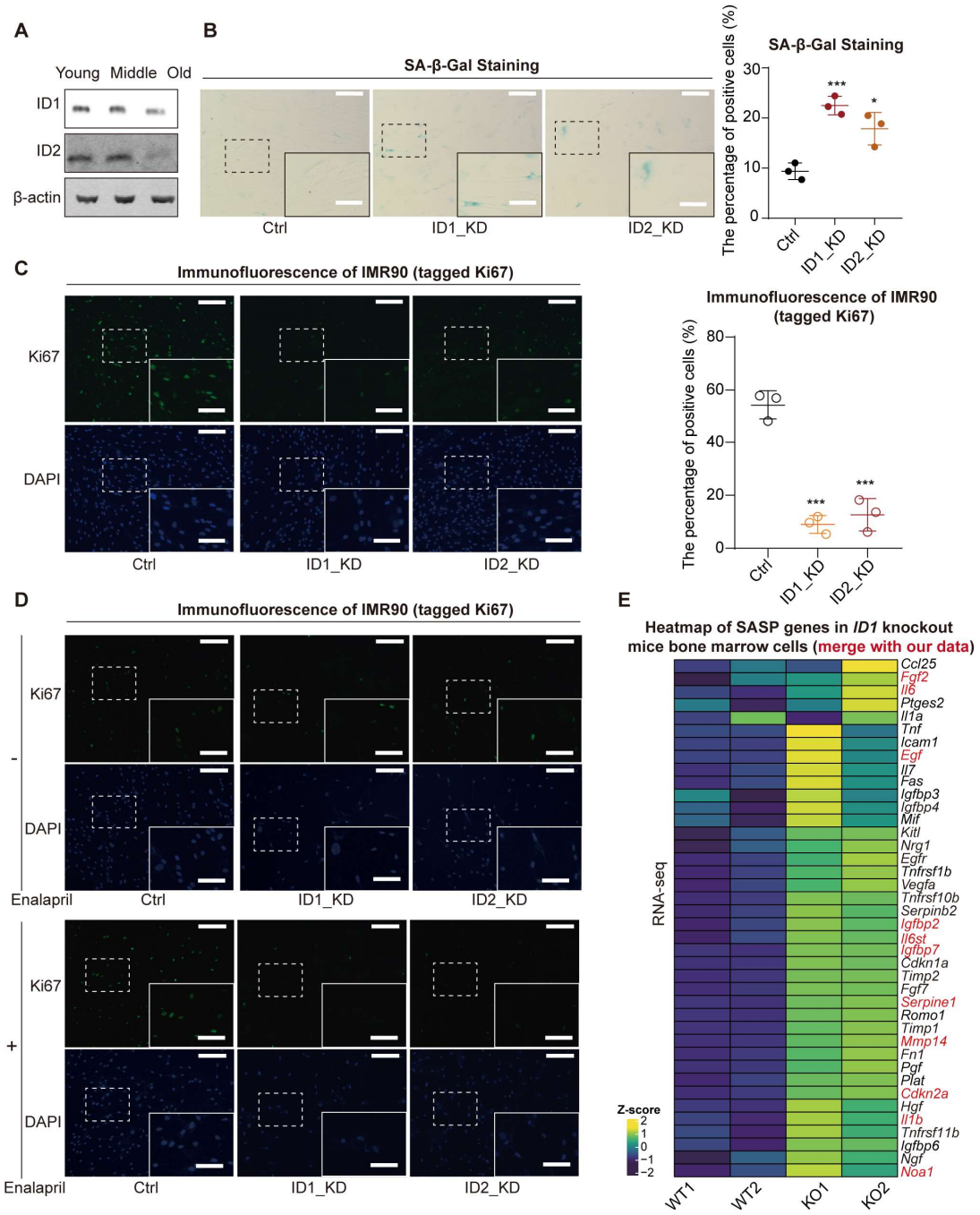

Figure S5 Knockdown of *ID* accelerates cellular senescence. (**A**) Western blot showing changes in ID protein levels during cellular senescence. (**B**) SA-β-Gal staining (left) following knockdown of *ID1* and *ID2*, along with corresponding statistical chart (right). Scale bars, 200 μm. Enlarged scale bars, 100 μm. (**C**) Ki67 immunofluorescence (left) following knockdown of *ID1* and *ID2*, along with corresponding statistical chart (right). Scale bars, 80 μm. Enlarged scale bars, 40 μm. A two-tailed t-test was employed, $*p < 0.05$, $***p < 0.001$. (**D**) Ki67 immunofluorescence in control group (Ctrl) and *ID* knockdown groups (ID1_KD, ID2_KD), with or without enalapril treatment. Scale bars, 80 μm. Enlarged scale bars, 40 μm. (**E**) Heatmap of SASP factor expression in mouse bone marrow cells following *ID* knockout from previously reported data(Fei et al., 2023).

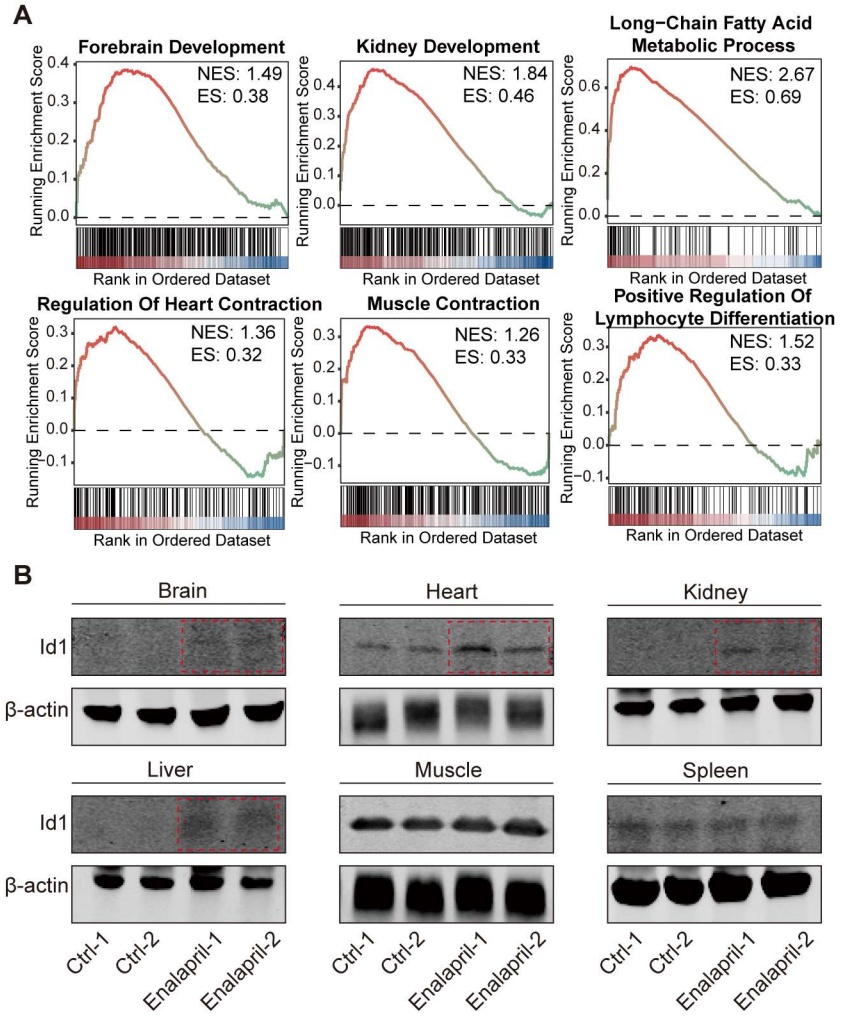

Figure S6 Effects of enalapril on the expression changes of genes related to organ

physiological functions in mice. (**A**) In multiple organs, enalapril increases the enrichment of GSEA pathways associated with improved physiological function. (**B**) Western blot analysis showing changes in Id1 protein levels in various organs of mice.

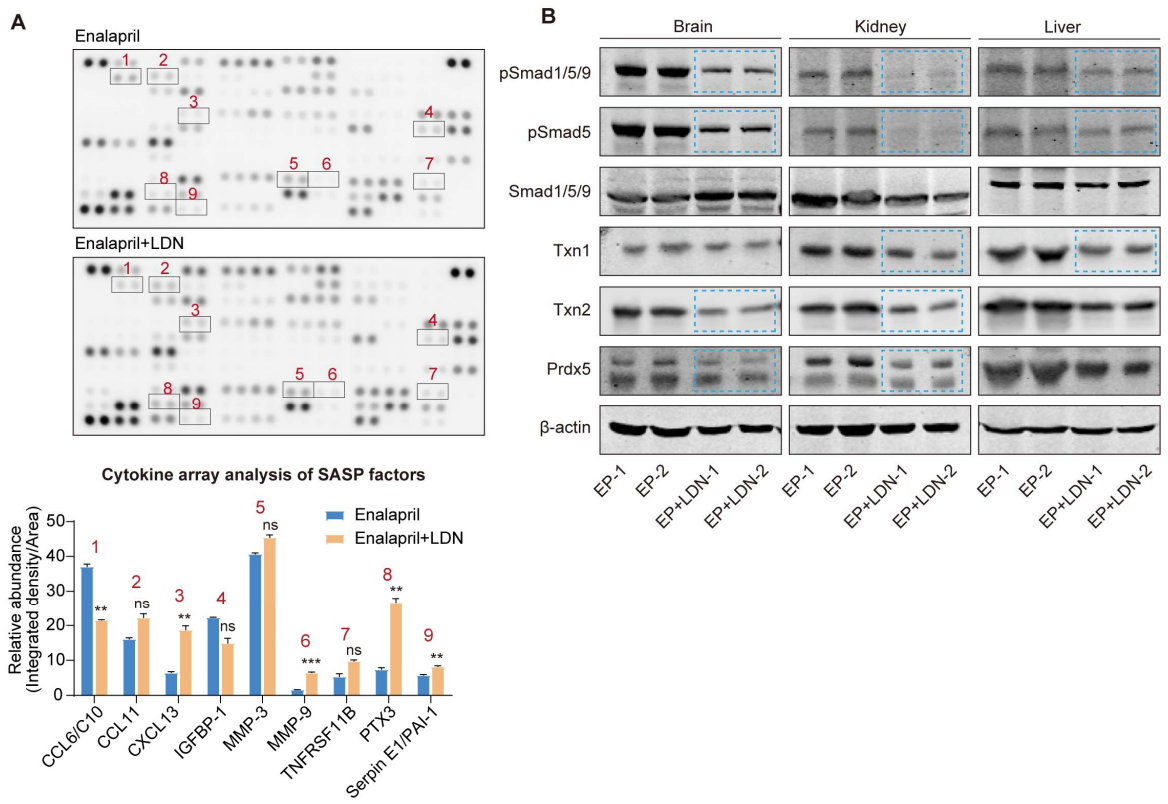

Figure S7 Effects of reduced pSmad1/5/9 levels on the expression changes of genes in mice. (**A**) Cytokine array analysis of secreted proteins (above) and relative quantitation (below) of SASP factors in enalapril-treated serum (Enalapril) and co-treated serum (Enalapril+LDN). (**B**) Western blot analysis showing the protein levels of pSmad1/5/9 and antioxidative genes in various organs following enalapril and LDN co-treatment.

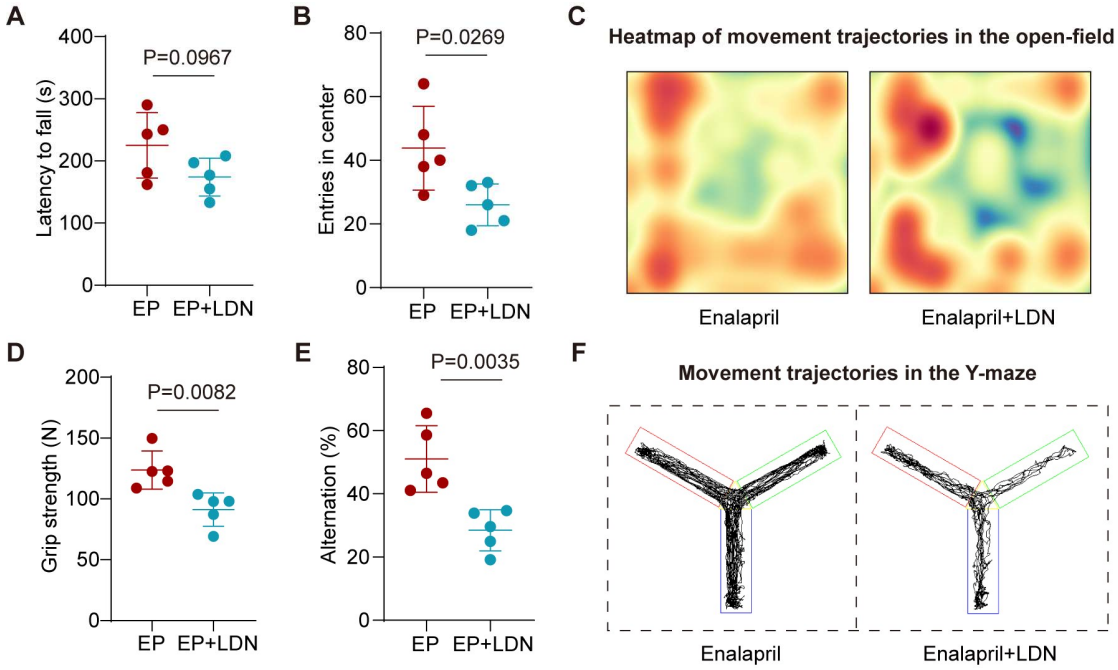

Figure S8 Effects of reduced pSmad1/5/9 levels on aging-related behaviors in mice. (**A, D**) Changes in the rotarod fall time (**A**) and grip strength (**D**) of the mice after enalapril and LDN treatment. (**B, C**) The number of entries into the central area (**B**) and heatmap of movement trajectories (**C**) in the open-field test after enalapril and LDN treatment. (**E, F**) Spontaneous alternation rate (**E**) and movement trajectory (**C**) in the Y-maze of the mice after enalapril and LDN treatment.

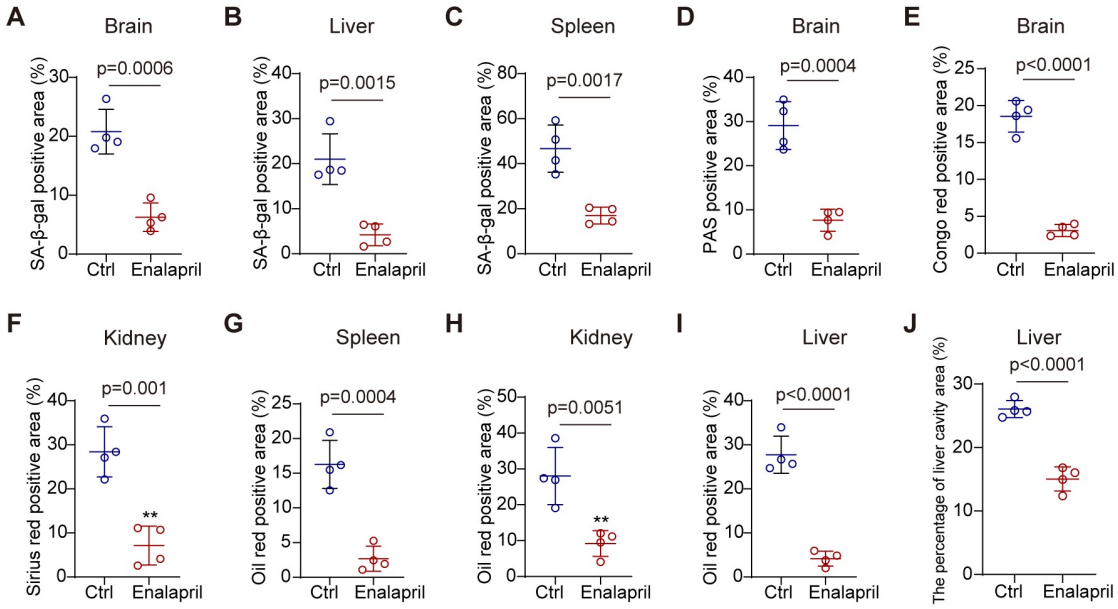

Figure S9 Enalapril ameliorates pathological phenotypes in aged mice. (**A-C**) SA-

β-Gal staining quantification chart of the brain (**A**), liver (**B**) and spleen (**C**) after enalapril treatment. (**D, E**) Periodic Acid-Schiff (PAS) staining (**D**) and Congo red staining (**E**) quantification chart of the brain after enalapril treatment. (**F**) Sirius red staining quantification chart of the kidney after enalapril treatment. (**G-I**) Oil Red O staining quantification chart of the spleen (**G**), kidney (**H**) and liver (**I**) after enalapril treatment. (**J**) Hematoxylin and eosin (H&E) staining quantification chart of the liver after enalapril treatment.

References

Fei, M. Y., Wang, Y., Chang, B. H., Xue, K., Dong, F. Y., Huang, D., . . . Wang, L. (2023). The non-cell-autonomous function of ID1 promotes AML progression via ANGPTL7 from the microenvironment. *Blood, 142*(10), 903-917. doi:10.1182/blood.2022019537

Morikawa, M., Koinuma, D., Tsutsumi, S., Vasilaki, E., Kanki, Y., Heldin, C. H., . . . Miyazono, K. (2011). ChIP-seq reveals cell type-specific binding patterns of BMP-specific Smads and a novel binding motif. *Nucleic Acids Res, 39*(20), 8712-8727. doi:10.1093/nar/gkr572

Sullivan, A. E., & Santos, S. D. M. (2020). An Optimized Protocol for ChIP-Seq from Human Embryonic Stem Cell Cultures. *STAR Protoc, 1*(2), 100062. doi:10.1016/j.xpro.2020.100062

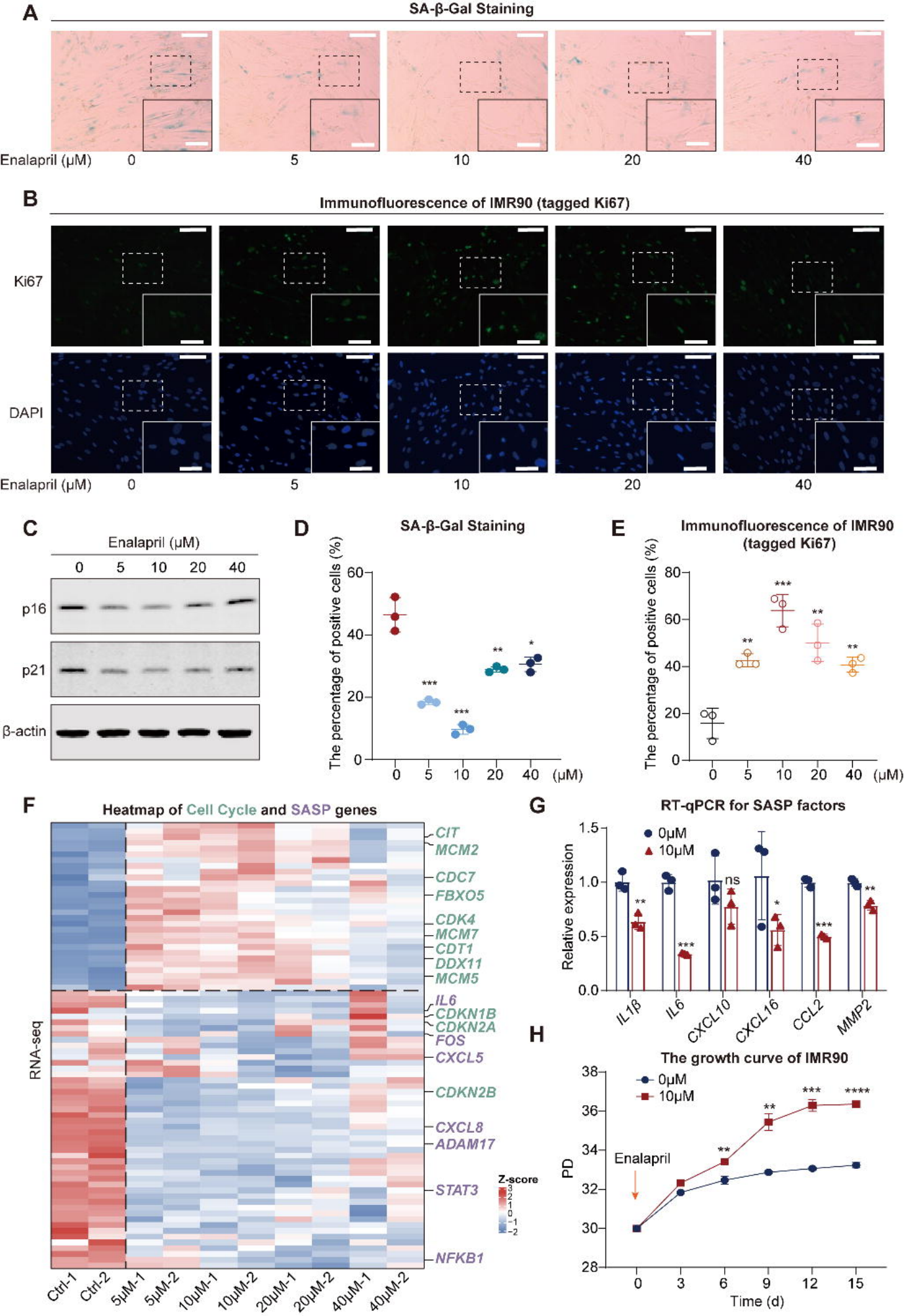
A
SA-β-Gal Staining
Enalapril (μM)
0
5
10
20
40
B
Immunofluorescence of IMR90 (tagged Ki67)
Ki67
DAPI
Enalapril (μM)
0
5
10
20
40
C
Enalapril (μM)
0 5 10 20 40
p16
p21
β-actin
D
SA-β-Gal Staining
The percentage of positive cells (%)
0
20
40
60
0 5 10 20 40 (μM)
***
***
**
*
E
Immunofluorescence of IMR90 (tagged Ki67)
The percentage of positive cells (%)
0
20
40
60
80
0 5 10 20 40 (μM)
**
***
**
**
F
Heatmap of Cell Cycle and SASP genes
RNA-seq
CIT
MCM2
CDC7
FBXO5
CDK4
MCM7
CDT1
DDX11
MCM5
IL6
CDKN1B
CDKN2A
FOS
CXCL5
CDKN2B
CXCL8
ADAM17
STAT3
NFKB1
Z-score
3
2
1
0
−1
−2
Ctrl-1
Ctrl-2
5μM-1
5μM-2
10μM-1
10μM-2
20μM-1
20μM-2
40μM-1
40μM-2
G
RT-qPCR for SASP factors
0μM
10μM
Relative expression
0.0
0.5
1.0
1.5
**
***
ns
*
***
**
IL1β
IL6
CXCL10
CXCL16
CCL2
MMP2
H
The growth curve of IMR90
0μM
10μM
Enalapril
PD
28
30
32
34
36
38
**
**
***
****
0 3 6 9 12 15
Time (d)

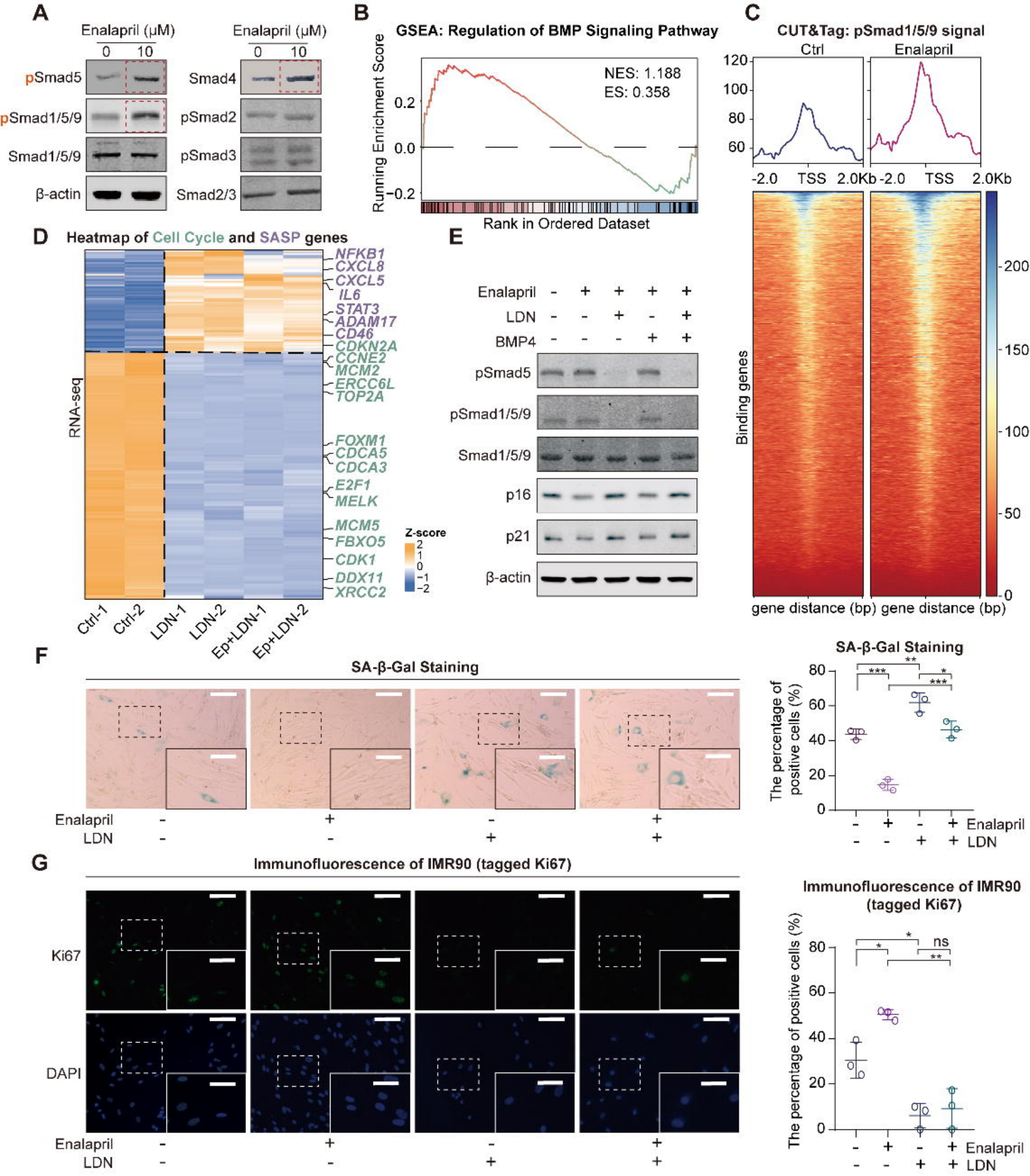
A
Enalapril (μM)
0
10
pSmad5
pSmad1/5/9
Smad1/5/9
β-actin
Smad4
pSmad2
pSmad3
Smad2/3
B
GSEA: Regulation of BMP Signaling Pathway
Running Enrichment Score
NES: 1.188
ES: 0.358
Rank in Ordered Dataset
C
CUT&Tag: pSmad1/5/9 signal
Ctrl
Enalapril
-2.0
TSS
2.0Kb
Binding genes
gene distance (bp)
D
Heatmap of Cell Cycle and SASP genes
RNA-seq
NFKB1
CXCL8
CXCL5
IL6
STAT3
ADAM17
CD46
CDKN2A
CCNE2
MCM2
ERCC6L
TOP2A
FOXM1
CDCA5
CDCA3
E2F1
MELK
MCM5
FBXO5
CDK1
DDX11
XRCC2
Z-score
Ctrl-1
Ctrl-2
LDN-1
LDN-2
Ep+LDN-1
Ep+LDN-2
E
Enalapril
LDN
BMP4
pSmad5
pSmad1/5/9
Smad1/5/9
p16
p21
β-actin
F
SA-β-Gal Staining
Enalapril
LDN
The percentage of positive cells (%)
G
Immunofluorescence of IMR90 (tagged Ki67)
Ki67
DAPI
Enalapril
LDN
The percentage of positive cells (%)

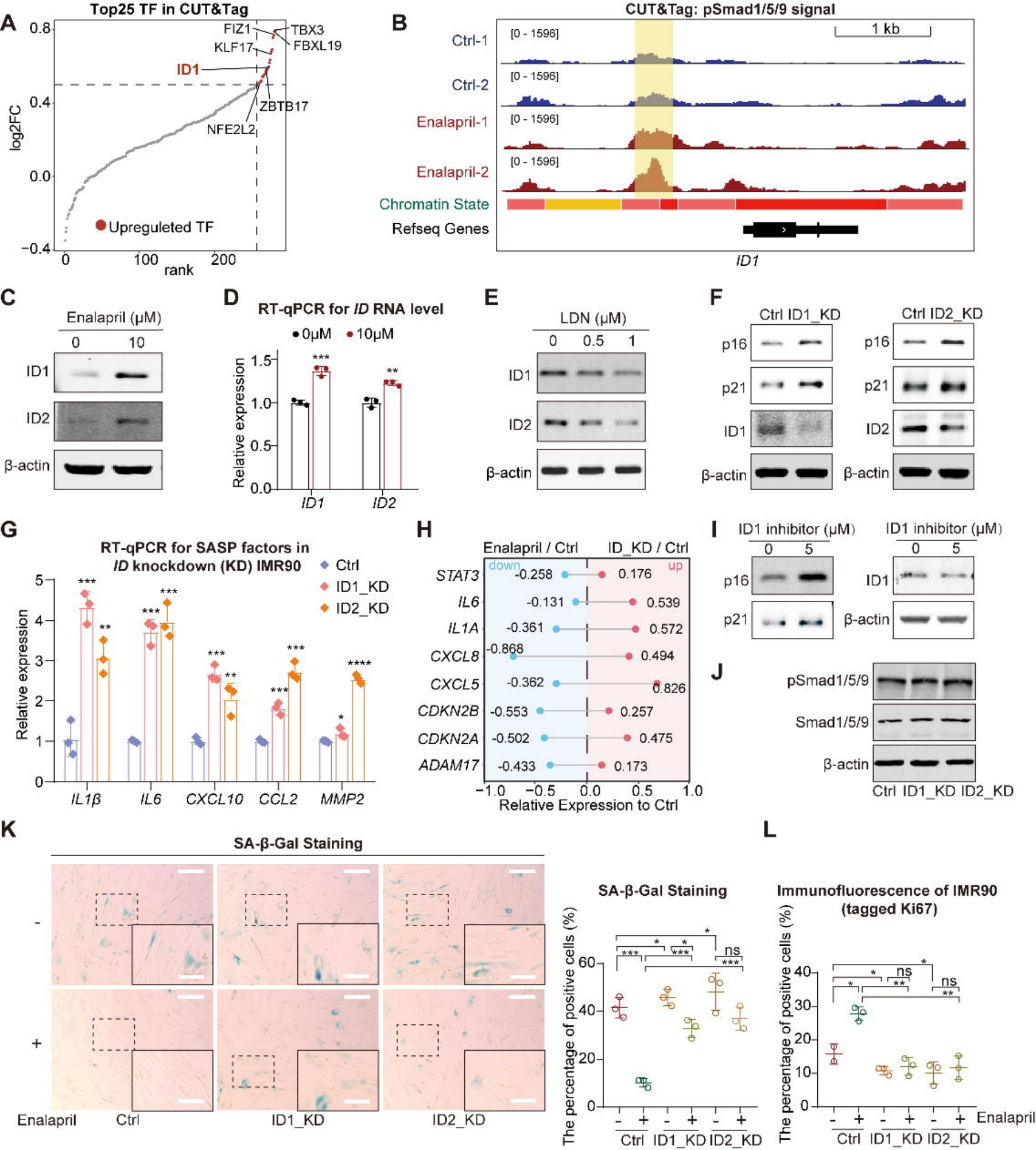
A
Top25 TF in CUT&Tag
FIZ1
TBX3
FBXL19
KLF17
ID1
ZBTB17
NFE2L2
Upreguleted TF
log2FC
rank
B
CUT&Tag: pSmad1/5/9 signal
Ctrl-1
Ctrl-2
Enalapril-1
Enalapril-2
[0 - 1596]
1 kb
Chromatin State
Refseq Genes
ID1
C
Enalapril (μM)
0
10
ID1
ID2
β-actin
D
RT-qPCR for ID RNA level
0μM
10μM
Relative expression
ID1
ID2
E
LDN (μM)
0
0.5
1
ID1
ID2
β-actin
F
Ctrl ID1_KD
Ctrl ID2_KD
p16
p21
ID1
ID2
β-actin
G
RT-qPCR for SASP factors in ID knockdown (KD) IMR90
Ctrl
ID1_KD
ID2_KD
Relative expression
IL1β
IL6
CXCL10
CCL2
MMP2
H
Enalapril / Ctrl
ID_KD / Ctrl
down
up
STAT3 -0.258 0.176
IL6 -0.131 0.539
IL1A -0.361 0.572
CXCL8 -0.868 0.494
CXCL5 -0.362 0.826
CDKN2B -0.553 0.257
CDKN2A -0.502 0.475
ADAM17 -0.433 0.173
Relative Expression to Ctrl
I
ID1 inhibitor (μM)
0
5
p16
p21
ID1
β-actin
J
pSmad1/5/9
Smad1/5/9
β-actin
Ctrl
ID1_KD
ID2_KD
K
SA-β-Gal Staining
Enalapril
Ctrl
ID1_KD
ID2_KD
SA-β-Gal Staining
The percentage of positive cells (%)
L
Immunofluorescence of IMR90 (tagged Ki67)
The percentage of positive cells (%)
Enalapril

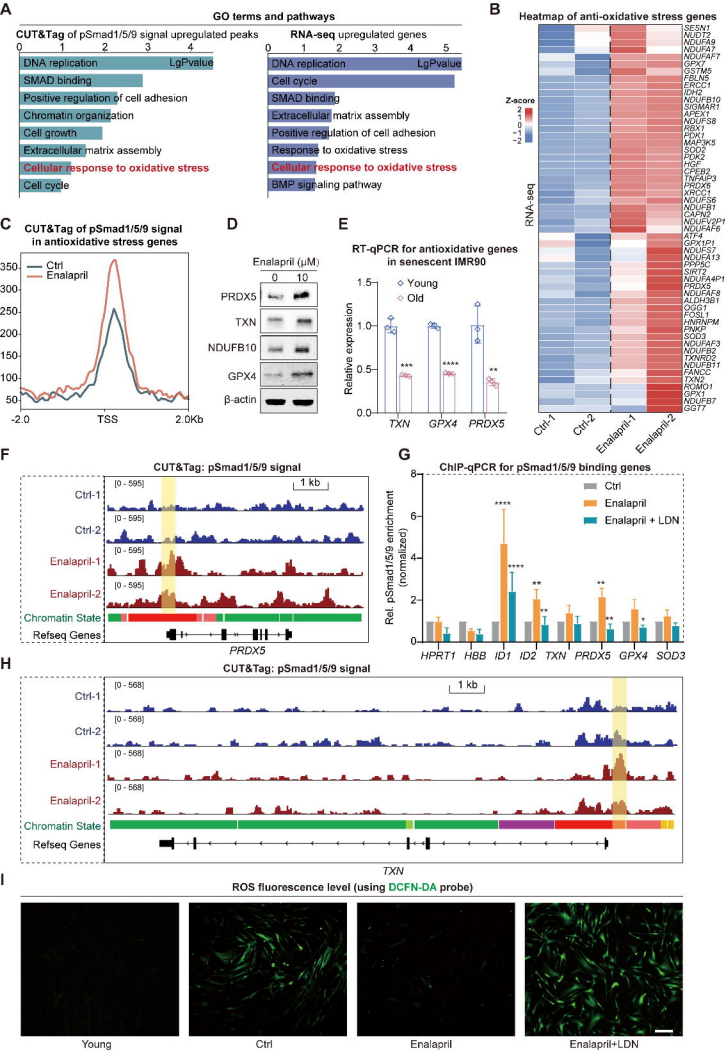
A
GO terms and pathways
CUT&Tag of pSmad1/5/9 signal upregulated peaks
0 1 2 3 4
DNA replication LgPvalue
SMAD binding
Positive regulation of cell adhesion
Chromatin organization
Cell growth
Extracellular matrix assembly
Cellular response to oxidative stress
Cell cycle
RNA-seq upregulated genes
0 1 2 3 4 5
DNA replication LgPvalue
Cell cycle
SMAD binding
Extracellular matrix assembly
Positive regulation of cell adhesion
Response to oxidative stress
Cellular response to oxidative stress
BMP signaling pathway
B
Heatmap of anti-oxidative stress genes
Z-score
2
1
0
−1
−2
RNA-seq
SESN1
NUDT2
NDUFA9
NDUFA7
NDUFAF7
GPX7
GSTM5
FBLN5
ERCC1
IDH2
NDUFB10
SIGMAR1
APEX1
NDUFS8
RBX1
PDK1
MAP3K5
SOD2
PDK2
HGF
CPEB2
TNFAIP3
PRDX6
XRCC1
NDUFS6
NDUFB1
CAPN2
NDUFV2P1
NDUFAF6
ATF4
GPX1P1
NDUFS7
NDUFA13
PPP5C
SIRT2
NDUFA4P1
PRDX5
NDUFAF8
ALDH3B1
OGG1
FOSL1
HNRNPM
PNKP
SOD3
NDUFAF3
NDUFB2
TXNRD2
NDUFB11
FANCC
TXN2
ROMO1
GPX1
NDUFB7
GGT7
Ctrl-1
Ctrl-2
Enalapril-1
Enalapril-2
C
CUT&Tag of pSmad1/5/9 signal in antioxidative stress genes
Ctrl
Enalapril
350
300
250
200
150
100
50
-2.0
TSS
2.0Kb
D
Enalapril (μM)
0 10
PRDX5
TXN
NDUFB10
GPX4
β-actin
E
RT-qPCR for antioxidative genes in senescent IMR90
Young
Old
Relative expression
1.5
1.0
0.5
0.0
***
****
**
TXN
GPX4
PRDX5
F
CUT&Tag: pSmad1/5/9 signal
1 kb
[0 - 595]
Ctrl-1
Ctrl-2
Enalapril-1
Enalapril-2
Chromatin State
Refseq Genes
PRDX5
G
ChIP-qPCR for pSmad1/5/9 binding genes
Ctrl
Enalapril
Enalapril + LDN
Rel. pSmad1/5/9 enrichment (normalized)
8
6
4
2
0
****
****
**
**
**
**
*
HPRT1
HBB
ID1
ID2
TXN
PRDX5
GPX4
SOD3
H
CUT&Tag: pSmad1/5/9 signal
1 kb
[0 - 568]
Ctrl-1
Ctrl-2
Enalapril-1
Enalapril-2
Chromatin State
Refseq Genes
TXN
I
ROS fluorescence level (using DCFN-DA probe)
Young
Ctrl
Enalapril
Enalapril+LDN

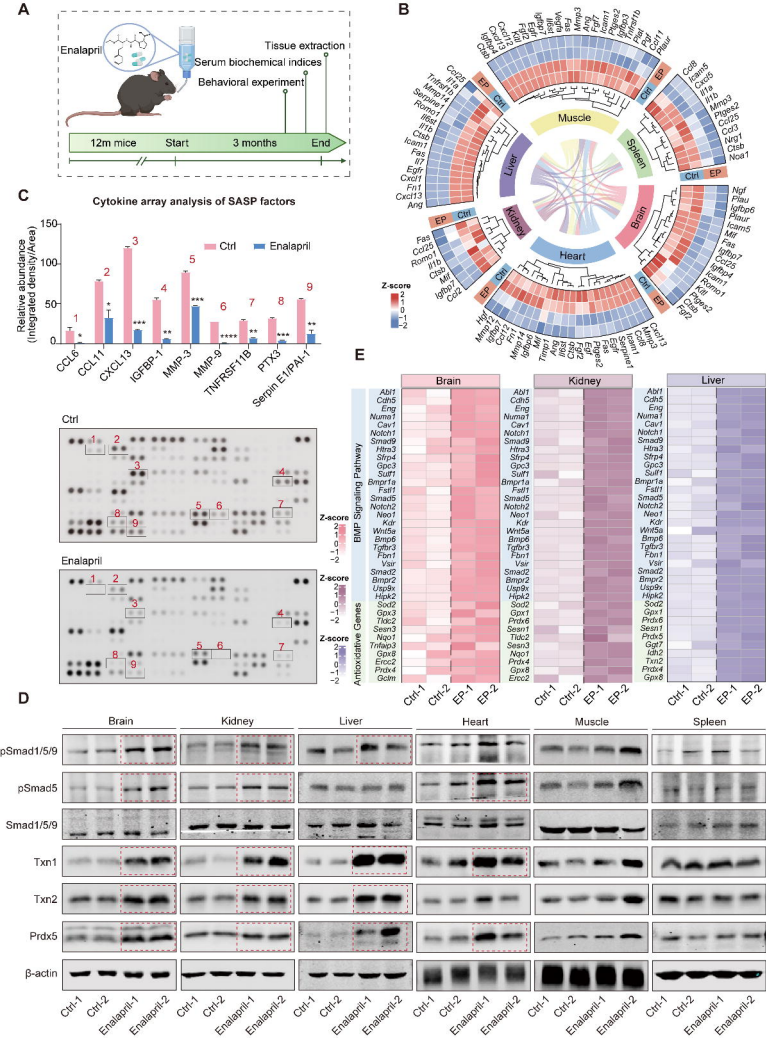
A
Enalapril
Tissue extraction
Serum biochemical indices
Behavioral experiment
12m mice
Start
3 months
End
B
Muscle
Spleen
Liver
Kidney
Brain
Heart
Ctrl
EP
Z-score
C
Cytokine array analysis of SASP factors
Relative abundance (Integrated density/Area)
Ctrl
Enalapril
CCL6
CCL11
CXCL13
IGFBP-1
MMP-3
MMP-9
TNFRSF11B
PTX3
Serpin E1/PAI-1
Ctrl
Enalapril
D
Brain
Kidney
Liver
Heart
Muscle
Spleen
pSmad1/5/9
pSmad5
Smad1/5/9
Txn1
Txn2
Prdx5
β-actin
Ctrl-1
Ctrl-2
Enalapril-1
Enalapril-2
E
Brain
Kidney
Liver
BMP Signaling Pathway
Antioxidative Genes
Z-score
Ctrl-1
Ctrl-2
EP-1
EP-2

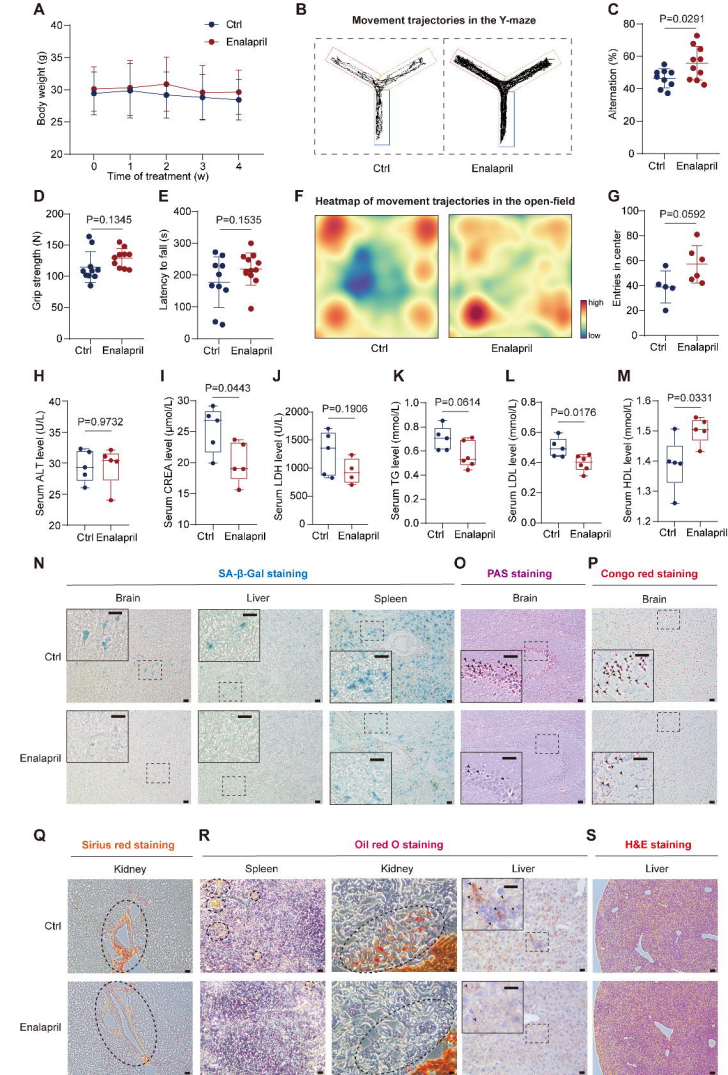
A
Ctrl
Enalapril
Body weight (g)
Time of treatment (w)
B
Movement trajectories in the Y-maze
Ctrl
Enalapril
C
P=0.0291
Alternation (%)
Ctrl
Enalapril
D
P=0.1345
Grip strength (N)
Ctrl
Enalapril
E
P=0.1535
Latency to fall (s)
Ctrl
Enalapril
F
Heatmap of movement trajectories in the open-field
high
low
Ctrl
Enalapril
G
P=0.0592
Entries in center
Ctrl
Enalapril
H
P=0.9732
Serum ALT level (U/L)
Ctrl
Enalapril
I
P=0.0443
Serum CREA level (μmol/L)
Ctrl
Enalapril
J
P=0.1906
Serum LDH level (U/L)
Ctrl
Enalapril
K
P=0.0614
Serum TG level (mmol/L)
Ctrl
Enalapril
L
P=0.0176
Serum LDL level (mmol/L)
Ctrl
Enalapril
M
P=0.0331
Serum HDL level (mmol/L)
Ctrl
Enalapril
N
SA-β-Gal staining
Brain
Liver
Spleen
Ctrl
Enalapril
O
PAS staining
Brain
P
Congo red staining
Brain
Q
Sirius red staining
Kidney
R
Oil red O staining
Spleen
Kidney
Liver
S
H&E staining
Liver
Ctrl
Enalapril

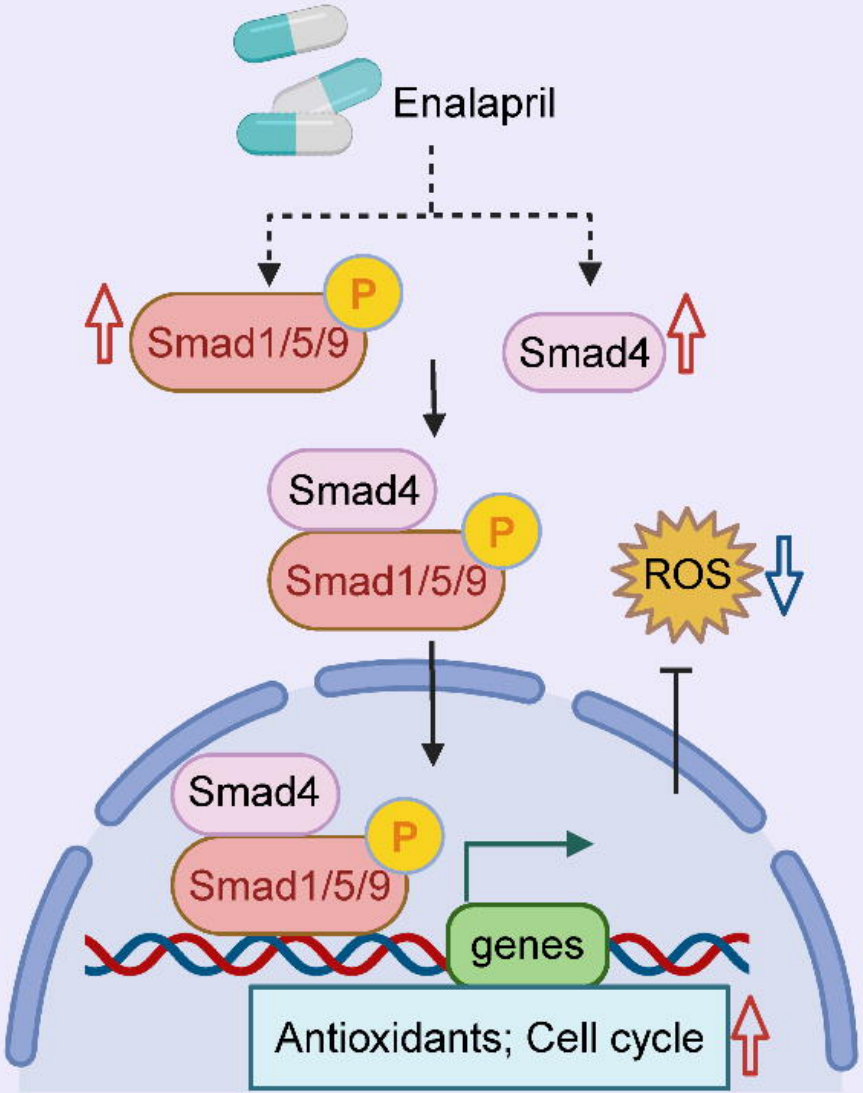

Mitigating age-related degenerative changes
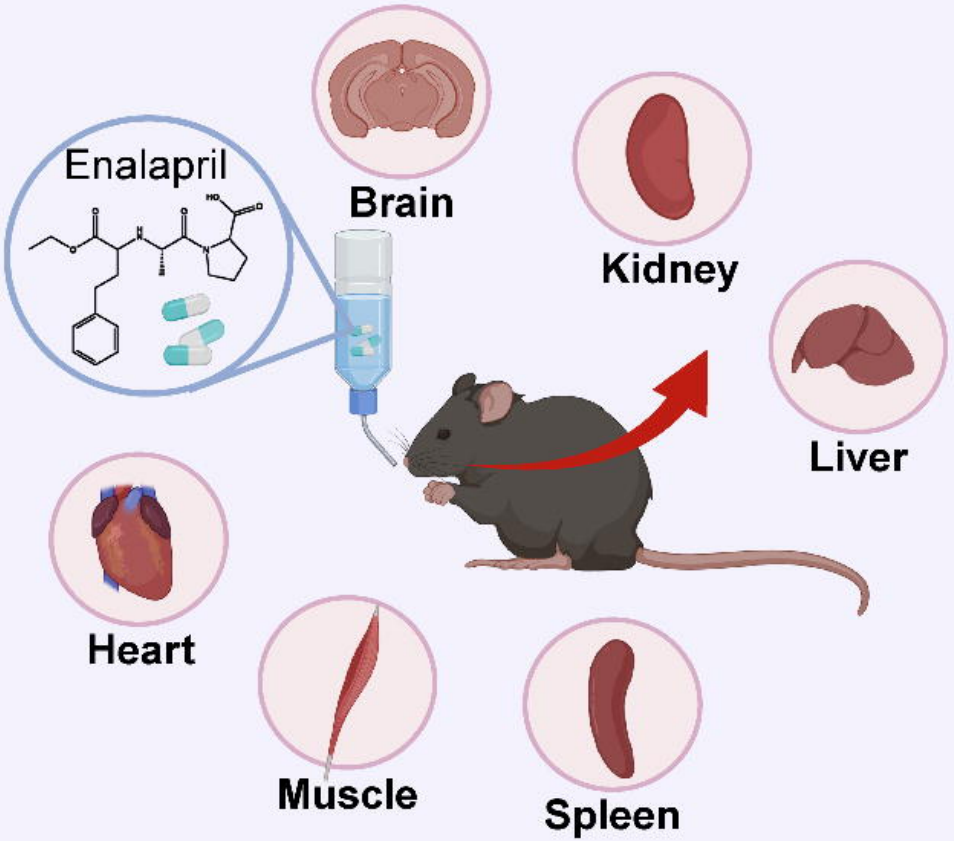
Enhanced memory, kidney development, liver metabolism, myocardial function, muscle endurance, reduced inflammation...